R. & M. No. 3466

MINISTRY OF TECHNOLOGY

AERONAUTICAL RESEARCH COUNCIL

The Effects of Base Bleed on Plug Nozzles

By J. Reid

LONDON: HER MAJESTY'S STATIONERY OFFICE
1967
PRICE £1 0*s.* 0*d.* NET

The Effects of Base Bleed on Plug Nozzles

By J. Reid

Reports and Memoranda No. 3466*
February, 1965

Summary.

This is an experimental comparison of two axi-symmetric, isentropic plug nozzles. In one of these (Model No. 1) the afterbody is cylindrical and a secondary flow is bled into the annular base. The other (Model No. 2) has a parabolic afterbody with no base or bleed. In both cases the expansion is all-external and the design pressure ratio is 14.

These models were tested over a range of primary and secondary flows at $M_\infty = 0$, 0·9 and 2·0. In the case of Model No. 1 measurements include the primary and secondary flow rates, the base pressure and the plug pressure distribution. The overall thrust was determined by a balance and analysed into its components; namely, the nozzle thrust and the drag of the bleed system. With Model No. 2 only the primary flow rate and overall thrust were measured.

Both nozzles are efficient at the cruising condition ($M_\infty = 2{\cdot}0$) and both are exceptionally flexible with regard to off-design operation ($M_\infty = 0{\cdot}9$ and 0). However, at $M_\infty = 0{\cdot}9$ and 2·0, the overall thrust of Model No. 1 using optimum bleed is slightly less than that of Model No. 2.

LIST OF CONTENTS

*Replaces R.A.E. Tech. Report No. 65 043—A.R.C. 27 137.

LIST OF CONTENTS—*continued*

---

1. *Introduction.*

In supersonic flight, as a result of the relatively low lift/drag ratio and high net specific fuel consumption, the payload is very sensitive to the efficiency of the propelling nozzle. In a typical aircraft cruising at Mach 2.2, for example, a loss of 1 per cent in nozzle efficiency decreases the payload by about 8 per cent. For this reason a high nozzle efficiency at the cruising speed is vital in such aircraft. However, other critical phases occur during the flight when a high nozzle efficiency is desirable. These include the stand-off condition at high subsonic speed, acceleration through the transonic speed range where the aircraft drag coefficient is large, and the initial phase of take-off in order to reduce noise levels in the neighbourhood of the airport. In supersonic aircraft, therefore, the propelling nozzle should operate efficiently over a wide range of flight speed and jet pressure ratio.

Now, the simple convergent-divergent expansion nozzle with fixed geometry is efficient when discharging into quiescent air at the design pressure ratio, but a reduction in the applied pressure ratio causes a loss in thrust due to over-expansion and, eventually, internal separation. Further, at low jet pressure ratios, an external stream reduces the pressure in the separated region and hence increases the loss in thrust. This type of behaviour is, indeed, characteristic of any nozzle in which the flow must either expand through a fixed area ratio, or separate. It can, of course, be avoided by mechanical variation of the nozzle geometry, but this is difficult to achieve and leads, in any case, to an increase in weight, and an increase in external drag when the jet pressure ratio is low.

Attention has therefore been directed to aerodynamic methods of adjusting the expansion ratio of the nozzle to suit the applied pressure ratio, and two distinct lines of reasoning based on this principle have been pursued. One of these leads to the aerodynamic or ejector nozzle[1], in which the primary flow from the engine is partly expanded in a nozzle of fixed geometry, and is then supplemented by a comparatively small and unheated secondary flow, normally derived from the free stream or the intake boundary-layer bleed. The combined streams are discharged through a shroud so that the effective expansion ratio of the primary flow is determined by the stagnation pressure of the secondary flow. The alternative approach, which leads to nozzles of the plug type, is examined in some detail below.

2. *Plug Nozzles and their Mode of Action.*

A typical axi-symmetric plug nozzle, operating at the design pressure ratio and discharging into still air, is represented in Fig. 1. In this design, expansion of the sonic flow at the nozzle throat (AB) is brought about by a simple expansion fan focussed on the cowl lip. The final characteristic (AC) of this fan passes through the apex of the plug. The static pressure decreases over the whole length of the plug and the flow is discharged parallel to the axis of symmetry, at uniform velocity and atmospheric pressure (p_∞). Outside the boundary layers the expansion process is essentially isentropic so that, under the stated conditions, the nozzle develops practically the maximum possible thrust.

In Fig. 1 the Mach number at the start of the expansion fan has been taken as unity. This is not an essential restriction since, in principle, the approach Mach number may assume any value between unity and the discharge value. For any given design pressure ratio there exists, therefore, a family of plug nozzles in which the degree of internal expansion varies from member to member. In this more general context the limiting case shown in Fig. 1 is usually distinguished by the prefix 'external expansion'. Since, however, only nozzles of this type will be considered henceforth, they will be referred to simply as 'plug nozzles'.

We consider next a plug nozzle discharging into still air at a jet pressure ratio ($_tp_1/p_\infty$ in Fig. 1) which differs from the design pressure ratio. Fig. 2a corresponds to the case when $_tp_1/p_\infty$ is greater than the design value. The free streamline then diverges from the axis and, typically, a shock wave is formed in the flow. The last characteristic of the expansion fan (AC) intersects the axis downstream of the plug vertex so that the minimum static pressure acting on the plug is greater than p_∞. Some thrust is therefore lost due to under-expansion, but this loss is relatively small. Under these conditions the behaviour of the plug nozzle is similar to that of a conventional convergent-divergent nozzle.

Of much greater practical importance is the performance at jet pressure ratios appreciably less than the design value (Fig. 2b). The free streamline is then inclined, initially, towards the axis and the final characteristic of the expansion fan (AC) intersects the plug surface well upstream of the apex. Downstream of C, curvature of the plug surface results in compression of the flow. The static pressure on the surface of the plug therefore decreases virtually* to p_∞ at C and then increases. Thereby, over-expansion with its attendant loss in thrust is eliminated. The efficiency of a plug nozzle discharging into still air is thus practically independent of jet pressure ratio, a result which has been amply confirmed by experiment[2-5].

An external stream of high subsonic or supersonic velocity interferes with the nozzle flow and a more complex field results, as shown in Fig. 3. Two points should be noted here. Firstly, the external flow separates from the cowl at a point (G) upstream of the lip (A), thus producing a region (AGF) of separated flow. The static pressure (p_B) of this separated region is less than p_∞ so that the nozzle always over-expands. Secondly, whatever the jet pressure ratio, a shock system (FE) traverses the nozzle flow.

We will assume provisionally that the point E lies downstream of the plug vertex (D). If then the jet pressure ratio is equal to or greater than the design value, over-expansion will not affect the static pressure distribution along the plug, and the nozzle thrust will be the same with external flow as without. On the other hand, if the jet pressure is less than the design value, the static pressure on the plug will decrease to $p_B < p_\infty$ (at C) before compression commences. (Compare Figs. 2b and 3). Consequently, a section of the plug will be subjected to a drag force (corresponding to the shaded area of the graph in Fig. 3), and the nozzle thrust will be less with external flow than without. With external flow, therefore, the efficiency of the nozzle decreases when the jet pressure ratio drops below the design value, and this loss is supplemented by the cowl drag. The importance of this effect depends on the nozzle geometry and operating conditions, and experimental work[6] suggests that for a typical turbojet installation at $M_\infty = 2$ the loss is not excessive. It is, however, clearly undesirable and could be reduced if means were available for increasing the base pressure (p_B).

Fortunately, one practical method of achieving this end is known and has been investigated experimentally[7]. With this method, usually referred to as 'base bleed', a relatively small amount of low-energy air is discharged through the base. The eddy system in the separated region is thereby destroyed and the

*The flow being axi-symmetric, the characteristics are, in general, curved and the flow parameters vary slightly along each characteristic.

base pressure substantially increased. This method is not ideal in that the optimum base pressure results when the exit velocity of the secondary 'bleed' flow is small. Additional losses are therefore incurred by the decrease in momentum of the secondary flow. Nevertheless, it would seem that the performance of the simple plug nozzle (Fig. 3) with external flow might be improved by surrounding the cowl with a cylindrical shroud and injecting a secondary flow into the base annulus.

A plug nozzle with base bleed of this type is sketched in Fig. 4. When operating at a low jet pressure ratio with external flow and base bleed the overall thrust developed by this nozzle depends on several factors. Firstly, the increase in p_B produced by the bleed flow will reduce over-expansion in the nozzle and hence increase the nozzle thrust. It will also decrease the base drag. On the other hand, the loss in momentum of the bleed air between the entry and exit of the secondary duct introduces additional drag. Moreover, the base drag without bleed is greater than the cowl drag of the simple plug nozzle.

Thus although, in principle, the idea looks promising it is difficult to decide, on general grounds, whether any worth-while advantage is likely to result from the use of base bleed with a plug nozzle. To resolve this point a simple plug nozzle (Fig. 3) and a plug nozzle with base bleed (Fig. 4), both with the same design pressure ratio, were made and tested at $M_\infty = 0$, 0·9 and 2·0. The results of this experiment form the basis of the present report.

3. *Experimental Apparatus.*

3.1. *The Models.*

The notation used with the two models tested is shown in Figs. 5a and b and in the 'List of Symbols'.

The major part of the experimental work was concerned with Model No. 1, an axi-symmetric isentropic plug nozzle with a cylindrical afterbody and base bleed. A detailed drawing of this model is shown in Fig. 6, and the exact values of the design parameters are given below.

Model No. 1.

$$\bar{\beta} = 36{\cdot}00°$$

$$\bar{M} = 2{\cdot}369 \qquad \bar{\mu} = 24{\cdot}97°, \qquad \overline{({}_tp_1/p_\infty)} = 13{\cdot}94$$

$$a_{th}/a_0 = 0{\cdot}2750, \qquad a_{e1}/a_0 = 0{\cdot}6424, \qquad a_{e1}/a_{th} = 2{\cdot}336.$$

In choosing these parameters it was assumed that, for a typical turbo-jet engine operating at $M_\infty = 2{\cdot}0$, ${}_tp_1/p_\infty = 14$ and a_{e1}/a_0 (without bleed) = 0·70. The design pressure ratio for Model No. 1 was therefore taken as 14, but a_{e1}/a_0 was decreased to 0·64 to accommodate a bleed duct of adequate area.

Of the various features which merit comment, we will consider first the design of the supersonic part of the plug. For this purpose we refer to Fig. 5a and assume that $\overline{({}_tp_1/p_\infty)}$, a_0 and a_{e1} are given. The plug vertex (C) is taken as a datum point. It is then apparent that the position of the cowl lip (A) is determined, together with the inclination ($\bar{\beta}$) of the tangent at A to the axis. We now take a straight line (AB) perpendicular to this tangent and assume that the velocity at any point on AB is sonic and normal to AB. The position (B) of the sonic point on the plug and the inclination ($\bar{\beta}$) of the tangent at B to the axis are then determined also.

Starting at AC, and noting that the flow at the singular point (A) is of Prandtl-Meyer type, a characteristics network was then constructed by numerical integration of the axi-symmetric characteristics equations. This calculation was terminated at a low supersonic Mach number. On this basis the plug contour, which coincides with the streamline through C, was constructed from C to a point (D) slightly downstream of the sonic point (B). B and D were then joined by a cubic curve giving continuity of the first derivative at its end points.

Since the cowl and the subsonic portion of the plug were given arbitrary parabolic contours, the assumptions made above with regard to the throat flow will not, in general, be admissible. Further, the characteristics mesh adopted was fairly coarse, and boundary-layer effects were ignored. The method outlined gives, therefore, only a first approximation to the true plug profile. Its justification in the present instance lies in previous work[2] which shows that, provided $\overline{\beta}$ and a_{e1}/a_{th} are correct, the thrust of a plug nozzle is insensitive to the shape of the plug.

A second point to note in Fig. 6 concerns the design of the bleed system. Originally it was intended to discharge the bleed flow through the full area of the annular base, as shown in Fig. 4. However, with this design the flow separated in the divergent bleed duct and the velocity in the base plane was not axi-symmetric; indeed, over quite large areas, flow reversal could be detected. Several attempts were made to improve the symmetry by fitting a wire gauze or baffle plates in the bleed plenum chamber, but these had little effect. A symmetrical discharge was finally achieved by a perforated base plate, as shown in Fig. 6. This plate introduces a loss in total pressure, but since the available total pressure is much greater than that required by the bleed, the performance of the system is not affected thereby. More serious is the reduction in bleed discharge area, a feature which detracts from the efficiency of base bleed, as previous work[7] has shown.

The second model tested, Model No. 2 which is shown in Fig. 7, is an axi-symmetric isentropic plug nozzle of the conventional type with a parabolic afterbody and no secondary flow. This model was designed with a nozzle area ratio (a_{e1}/a_0) of 0·70, slightly larger than that of Model No. 1 for the reasons already given. However, the design pressure ratio was the same [$(\overline{p_1/p_\infty}) = 14$], so that the two models are geometrically similar as regards the primary flow, and should have the same performance at $M_\infty = 0$. Since Model No. 2 was intended primarily as a reference nozzle with respect to thrust, no static pressure points were installed, either on the afterbody or the plug.

3.2. *The Wind Tunnel.*

The R.A.E. Jet Interference Tunnel shown in Fig. 8 was used for the experiment. This is a continuous free-jet tunnel designed specifically to minimize support interference in tests with mixed exhaust flows. To this end the tunnel nozzle is axi-symmetric and the model is supported in the working section by a cylindrical tube (the centrebody) which passes through the throat of the nozzle, and its settling chamber, into a separate plenum chamber, where it is connected to a slotted drum. This central assembly comprising the slotted drum, centrebody and model is supported by three sets of ball bearings and is free to slide axially between limit stops.

The thrust developed by the model can be measured either by a hydraulic balance or by weights. Experience has shown that the most accurate results are obtained when weights are used to balance the major part of the thrust and the remainder is absorbed hydraulically. With this technique, frequent calibration of the hydraulic balance over the full range of thrust is unnecessary. Further, since the equilibrium point does not move with change in thrust, spurious loads due to connecting pipes are eliminated. When the model is running at the design pressure ratio the balance is sensitive to 0·1 per cent of the measured thrust. The error in absolute measure is difficult to estimate but it is probably less than 0·5 per cent of the nozzle thrust under the same conditions.

Undried air at atmospheric temperature and a maximum pressure of 2 atm. abs. forms the primary air supply to the model. The primary mass flow is measured by a single axial pitot point and wall static installed in the centrebody. This flowmeter was calibrated carefully over a range of stagnation pressure and Mach number by pitot traverses. The calibration was checked by measuring the mass flow through several sonic nozzles at different stagnation pressures and comparing the measured discharge coefficients with published values. The results indicate that the error in mass flow measurement does not exceed 0·5 per cent.

The secondary (bleed) flow to the model, which is supplied from the compressed air main at atmospheric temperature and 7 atm. abs. pressure, is measured by observing the pressure difference across a shaped orifice operating at a constant supply pressure of 5 atm. abs. Since this metering orifice is of established design it was not calibrated. The secondary flow is delivered radially to the double-skinned centre-

body by a flexible pipe, and thence *via* eight plastic tubes to the model. Checks were made to ensure that the flexible pipe did not load the balance under the operating conditions.

Dry air at atmospheric temperature and a maximum stagnation pressure of 1 atm. abs. is supplied to the two axi-symmetric tunnel nozzles. The first of these was designed integrally with the centrebody to give a Mach number of 2·0. This nozzle, which has an exit diameter of 11 inches is run at approximately atmospheric stagnation pressure. The second nozzle is convergent with an exit diameter of 10 inches. This nozzle operates at subsonic Mach numbers up to 0·9. It is normally run at a stagnation pressure of 0·5 atm. abs. with the tunnel diffuser removed.

A full description of the jet interference tunnel has been published elsewhere[8].

4. *Analysis of Thrust Data.*

The notation and definitions used with respect to thrust and drag are given in Appendix A, and in Appendix B these definitions are applied to an analysis of the forces acting on an engine nacelle. The result of this analysis may be summarized thus.

If S_1 and S_2 are the primary and secondary nozzle thrusts, respectively;
D_1 and D_2 are the primary and secondary intake drags, respectively;
D_F is the forebody drag,
D_A is the afterbody drag,
and X is the resultant axial thrust on the nacelle (i.e. the force transmitted to the airframe).

Then,

$$X = (S_1+S_2)-(D_1+D_2+D_F+D_A).$$

If, however, we are comparing different installations of the same engine operating at given conditions, D_1 and D_F are invariant, so that

$$Y = (S_1+S_2)-(D_2+D_A)$$

is a direct measure of X. Our present object is to show how Y and its component parts are obtained from the experimental data. The method follows:

(1) In the experimental rig (Fig. 8) the primary and secondary nozzle flows are supplied radially to the centrebody. Hence the balance reading, corrected for the skin-friction drag of the centrebody and unbalanced pressures in the tunnel chambers, gives $(S_1+S_2-D_A)$.

[The centrebody skin-friction drag is determined in a preliminary experiment with the model removed and the centrebody sealed directly by a bluff base. Comparison of the balance reading with the integrated base-pressure distribution gives the skin-friction drag on the centrebody.]

(2) D_2 is calculated assuming that, in an actual engine installation, the secondary intake captures air from the free stream and operates under critical or super-critical conditions. On these assumptions $D_2 = Q_2 u_\infty$, and both Q_2 and u_∞ are measured quantities.

(3) S_1 is calculated in terms of the nozzle geometry, the jet pressure ratio, and the measured distribution of static pressure along the plug. Details of the analysis are given in Appendix C.

(4) The component of afterbody drag due to skin friction may safely be neglected. D_A is therefore determined by integration of the measured static-pressure distribution along the afterbody.

Steps (1) to (4) above serve to determine Y and its components S_1, S_2, D_2 and D_A for a model of general configuration with primary and secondary flows and an afterbody. However, the experimental models were limiting cases of this general configuration. Moreover, the complete analysis was not applied to the reference model (No. 2). The simplified procedure actually used may be summarized thus.

Model No. 1 $(D_A = 0)$
Step (1) gives S_1+S_2. Step (2) gives D_2. Step (3) gives S_1.
Hence $Y = S_1+S_2-D_2$ and its components are determined.

Model No. 2 $(D_2 = S_2 = 0)$
Step (1) gives $Y = S_1-D_A$. Further analysis, which would have required pressure points on the afterbody or plug, was considered unnecessary.

We note that, for Model No. 1, Y depends only on the balance reading and the convention adopted in step (2) with regard to the operating conditions of the secondary intake. On the other hand, S_1 is calculated (Appendix C) on the basis of five assumptions.

(i) The entire flow is axi-symmetric.

(ii) ${}_tp_1$ and ${}_tT_1$ are uniform across the section.

(iii) The subsonic flow is isentropic.

(iv) The sonic line is normal to the throat flow.

(v) The force on the plug due to skin friction is negligible.

Since these assumptions are not strictly valid in practice, we might expect an appreciable error in the calculated value of S_1. Fortunately, under certain restricted conditions, a direct check with the experimental data can be made. Thus, when $Q_2 = 0$ equation (B6) takes the simple form

$$S_2 = (p_B-p_\infty)\,a_{e2}$$

so that S_1 follows from the balance reading and the measured base pressure. Further, when $Q_2 = 0$ and $M_\infty = 0$, then $S_2 = 0$ so that the balance reading gives S_1 directly. This check was applied over a range of jet pressure ratio at $M_\infty = 0$, 0·9 and 2·0 and it was found that the average difference between the measured and calculated values of S_1 was about 0·5 per cent. This relatively close agreement is probably favoured by chance, in that errors arising from the various assumptions partly cancel.

In presenting the data, any force associated with a given nozzle is expressed non-dimensionally in terms of a reference thrust (S^*). Let Q_1 be the primary mass flow of the given nozzle, ${}_tp_1$ and ${}_tT_1$ the stagnation conditions in the jet pipe, and p_∞ the free-stream pressure. Then S^* is the thrust corresponding to isentropic expansion of mass flow Q_1 from uniform stagnation conditions ${}_tp_1$, ${}_tT_1$, to a uniform static pressure p_∞.

Thus we present the results in terms of a nozzle efficiency (η_N) and an overall efficiency (η_0) defined by:

$$\eta_N = \frac{S_1}{S^*}$$

$$\eta_0 = \frac{(S_1+S_2)-(D_2+D_A)}{S^*}.$$

Note that, for Model No. 1 $(D_A = 0)$, $\eta_0 = \dfrac{S_1+(S_2-D_2)}{S^*}$

and for Model No. 2 $(D_2 = S_2 = 0)$ $\eta_0 = \dfrac{S_1-D_A}{S^*}$.

Hence, with reference to S^*, η_N represents the nozzle thrust, η_0 the overall thrust, and $(\eta_N-\eta_0)$ the internal drag of the bleed system (Model No. 1) or the afterbody drag (Model No. 2). These efficiencies do not take into account either the forebody drag (D_F) or the primary intake drag (D_1).

5. *Preliminary Experiments.*

5.1. *Calibration of the subsonic Wind Tunnel Nozzle.*

Since, in previous work with the jet interference tunnel only the supersonic nozzle was used, calibration of the subsonic nozzle formed an essential preliminary to the present experiment. This calibration was done in two steps. In the first step the Mach number was measured along one generator of the centrebody and nozzle wall with the centrebody extending well downstream of the working section. With this configuration the Mach number distribution is not affected by disturbances at the base of the centrebody. Fig. 9 shows that at $M_\infty = 0{\cdot}7$, 0·8 and 0·9 the axial variation in Mach number is small, and further tests (not plotted) indicated that the flow was reasonably axi-symmetric. In Fig. 9 we may note that the local Mach number is calculated with reference to the stagnation pressure in the supply reservoir and the local wall static pressure, assuming isentropic flow.

In the jet interference tunnel the centrebody blockage (Fig. 10) is some 15 per cent, a value which is larger than is customary in tests at high subsonic speeds. It is therefore possible that the flow around the model is influenced by the proximity of the nozzle walls, and in this event the observed data will differ from those corresponding to actual flight, when the free stream is virtually infinite in extent. To check this point the pressure was measured on a bluff base at two axial stations within the working section over a range of Mach number. In Fig. 10 the results are compared with data obtained by Kurn[9] and by Cubbage[10] on similar configurations in relatively large transonic tunnels of accepted design.

We note first that there is close agreement between the results of Refs. 9 and 10 over the Mach number range and since, in both cases, the tunnel liner was slotted and the centrebody blockage small, these results presumably correspond to conditions in flight. However, in the jet interference tunnel the base pressure depends on the axial position of the base. Thus, when the base lies in the nozzle exit plane ($L = 17{\cdot}5$ in.), the base pressure at subsonic Mach numbers falls appreciably below the reference curve. In this position tunnel constraints are probably affecting the measurements. On the other hand, when the base is placed in the free jet downstream of the nozzle exit ($L = 23{\cdot}5$ in.), the base pressure curve lies reasonably close to the reference curve at subsonic Mach numbers. With this configuration it seems probable that the constant pressure boundary of the free jet acts in a similar manner to slots in a rigid liner, and hence reduces tunnel constraints. In the main experiment all subsonic tests were done at $M_\infty = 0{\cdot}9$ with $L = 23{\cdot}5$ in. and the evidence given above suggests that these results are not seriously affected by tunnel interference.

5.2. *The Effect of Water Vapour on the Primary Nozzle Thrust.*

Throughout the experiment the primary nozzle was supplied with undried air from the atmosphere at a stagnation temperature of about 20 deg C. Under these conditions, supersonic expansion in the primary nozzle may give rise to a weak condensation shock which would slightly increase the static pressure on the plug, and hence the primary nozzle thrust. This process cannot occur in the heated flow from a turbo-jet engine so that, to this extent, the experiment does not exactly simulate engine operating conditions.

To determine the magnitude of the effect, a day of average atmospheric humidity was chosen and two consecutive runs made with Model No. 2 at $M_\infty = 0$, using first dried air then undried air. Comparison of the results (Fig. 11) shows that an increase in absolute humidity from 0·0005 to 0·0065 increases the nozzle efficiency by about 0·5 per cent, regardless of the jet pressure ratio. Since this increment is of the same order as the absolute accuracy of the thrust data, the results presented in this Report have not been corrected for the effects of moisture in the primary flow.

5.3. *Boundary-Layer Data.*

Traverses showed that the boundary layer on the centrebody is turbulent and reasonably axi-symmetric both at $M_\infty = 0{\cdot}9$ and $M_\infty = 2{\cdot}0$. Values of the boundary-layer parameters, measured 0·5 in. upstream of the base plane of each model are given in Table 1.

TABLE 1

Centrebody Boundary-Layer Parameters.

M_∞	Displacement thickness δ^* (in.)	Momentum thickness θ (in)
0·9	0·031	0·020
2·0	0·045	0·015

No measurements were made of the boundary layer on the isentropic plug.

6. *The Main Experiment.*

6.1. *Tests with Model No.* 1.

At $M_\infty = 0$, corresponding to the take-off case, secondary flow is not used. The model was therefore tested with H_2 zero*, over a range of jet pressure ratio ($_tp_1/p_\infty$) from 2 to 20. At each condition observations were made of the balance reading, the primary mass flow and the pressure distribution on the plug.

In the subsonic tests at $M_\infty = 0{\cdot}9$ the model was tested with $_tp_1/p_\infty$ equal to 4, 6 and 8, and H_2 ranging from zero to 0·05. These data were supplemented by further observations with $_tp_1/p_\infty = 5$ and 7, and $H_2 = 0$. At each condition the balance reading was recorded, together with the primary and secondary mass flow, the base pressure and the plug pressures. The range of jet pressure ratio covered spans the likely operating region for a turbo-jet engine at this Mach number.

At $M_\infty = 2{\cdot}0$, the cruising Mach number, a full set of readings (balance, mass flows, base and plug pressures) was taken with $_tp_1/p_\infty$ equal to 6, 8, 10, 14 and 19, and H_2 ranging from zero to 0·025. In addition, the plug pressures only were measured with H_2 zero and $_tp_1/p_\infty$ equal to 3, 4, 5, 7 and 12.

Since, in this experiment, quite small differences in thrust are important, the experimental technique demanded considerable care. In general, M_∞ and $_tp_1/p_\infty$ were held constant during each run and the variation in thrust with respect to H_2 was measured. By repeating selected curves at intervals throughout the experiment it was shown that this procedure gave reliable and consistent results.

6.2. *Tests with Model No.* 2.

This model was tested at the same values of free stream Mach number and jet pressure ratio as Model No. 1. At each condition the thrust and primary mass flow were measured.

A comprehensive set of schlieren photographs was taken with both models.

7. *Results.*

7.1. *Results with Model No.* 1 *at* $M_\infty = 0$.

To check the design procedure we first consider the nozzle operating at the design pressure ratio ($_tp_1/p_\infty = 14$). Theory and experiment are compared in Fig. 12, which shows the distribution of static pressure along the plug, the characteristics diagram, and a schlieren photograph of the flow. The characteristics net was constructed on the assumption that the sonic line is straight and normal to the throat flow (Section 3.1). That this assumption is not strictly true is shown by Fig. 12 (bottom), which indicates that the sonic point on the plug actually lies slightly upstream of the assumed position. The nozzle therefore over-expands a little in the region of the throat, but further downstream theory and experiment are in good agreement. This local over-expansion also causes the free streamline leaving the cowl lip to diverge

*The secondary mass flow is expressed non-dimensionally in terms of the conventional bleed number (H_2) defined in the 'List of Symbols'.

slightly from the axis (Fig. 12, top). Typically, this initial divergence is corrected by a shock wave, which is weak near the cowl lip, but which strengthens as the axis is approached. This shock system does not intersect the plug and hence has no effect on the pressure distribution or the nozzle thrust. With these qualifications in mind, the nozzle behaves essentially in the predicted manner at the design point.

Fig. 13 presents similar data for the case when the operating pressure ratio ($_tp_1/p_\infty = 7$) is appreciably less than the design pressure ratio. Referring first to the characteristics diagram we note that initially the flow expands, as before, through a fan centred at the cowl lip. Under these conditions, however, the final characteristic (AC) of this fan intersects the plug well upstream of the vertex and subsequently the plug produces a region of compression. In this region the characteristics converge, but they do not form an envelope, so that in inviscid flow an isentropic compression process is compatible with the equations of motion. In practice, however, the adverse pressure gradient along the plug causes boundary-layer separation accompanied by shock compression, as is clearly shown by the schlieren photograph. This point is further illustrated by the plug pressure distribution (Fig. 13, bottom). The experimental and theoretical curves are of the same general form but the actual compression region is shorter than is predicted by inviscid theory.

Fig. 14a shows the effect of jet pressure ratio ($_tp_1/p_\infty$) on the plug pressure distribution, plotted in terms of $p/_tp_1$. Provided that $_tp_1/p_\infty \geqslant 14$ the plug pressure distribution is invariant with respect to jet pressure ratio because the plug lies wholly within the expansion fan centred on the cowl lip. On the other hand, when the jet pressure ratio is less than the design value, each curve branches off the parent curve where the final characteristic of the expansion fan intersects the plug surface. Shock compression follows, as described above, and the static pressure then decays relatively slowly to the ambient value. At the two lowest values of jet pressure ratio this decay is succeeded by re-compression.

In Fig. 14b the same data are plotted in terms of p/p_∞. (The curves for $_tp_1/p_\infty = 3$ and 4 tend to confuse the presentation and are omitted.) This graph serves to emphasise an important point; namely, that when the jet pressure ratio is less than the design value, the minimum static pressure on the plug is practically equal to the ambient pressure*. Thus, over-expansion is eliminated and, indeed, it is clear that when the jet pressure ratio is low, compression towards the rear of the plug contributes substantially to the total thrust. Additional evidence on the change in flow pattern with jet pressure ratio is provided by the sequence of schlieren photographs shown in Fig. 15.

The effect of jet pressure ratio on the nozzle efficiency is shown in Fig. 16. The experimental points on this graph were taken at four different values of the back pressure (p_∞) and, since Models No. 1 and 2 are geometrically similar as regards the primary flow (Section 3.1), results for both nozzles are included. As a result the experimental scatter is greater than would normally be expected but, nevertheless, the mean curve is defined within fairly close limits. Clearly, at $M_\infty = 0$, the performance of the models with regard to thrust is excellent, in that the nozzle efficiency is equal to 0·985 at the design point and is practically independent of jet pressure ratio. This is a characteristic, and most important, property of the plug nozzle which is not shared by any other design with fixed geometry.

7.2. *Results with Model No. 1 at* $M_\infty = 0{\cdot}9$.

When the ambient conditions are not static, the external stream affects the base pressure and primary nozzle flow unfavourably, and base bleed is used with the object of reducing this interference. We have, therefore, to investigate the effect of jet pressure ratio and base bleed on the base pressure, the plug pressure distribution and the thrust. Some ambiguity exists with regard to the choice of a parameter to represent the bleed mass flow. The simple ratio Q_2/Q_1, which has a direct practical significance, is sometimes used, but in the present Report the familiar bleed number (H_2) is preferred in that it helps to correlate the data. The definition of H_2 and its relation to Q_2/Q_1 are given in the 'List of Symbols'.

---

*Since the flow is axi-symmetric, the static pressure along each characteristic of the expansion fan is not constant, but increases slightly as the axis is approached.

Fig. 17 shows the effect of jet pressure ratio ($_tp_1/p_\infty$) and bleed number (H_2) on the base pressure ratio (p_B/p_∞). We note that when $_tp_1/p_\infty = 4$, H_2 has practically no effect on p_B/p_∞. As $_tp_1/p_\infty$ is increased the influence of base bleed becomes more apparent, but in no circumstances is the base pressure increased to anything approaching the free stream value. These data are confirmed by schlieren photographs (Fig. 18) which show that when $_tp_1/p_\infty = 6$ the flow pattern does not change with bleed number. In terms of the fundamental flow mechanism these results are difficult to interpret, since very little is known about base flow, with or without bleed, when the internal flow is supersonic and the external flow subsonic. However, it seems likely that base bleed is not being exploited to its full advantage with the present configuration. Since the practical implications are clearly disappointing, further research on this point might well be both interesting and profitable.

Fig. 19 shows the plug pressure distribution (plotted in terms of both $p/_tp_1$ and p/p_∞) at different values of jet pressure ratio. Each curve is independent of bleed number, for reasons which will shortly become apparent. Comparison of Fig. 19 (lower) with Fig. 17 (lower) shows that when $_tp_1/p_\infty = 4$, the flow expands until the plug pressure is virtually equal to the base pressure, and is then compressed. At this condition the flow is similar to that which exists when $M_\infty = 0$, except that the effective back pressure is p_B instead of p_∞. The top schlieren photograph in Fig. 20 illustrates the type of flow pattern. However, at the higher values of jet pressure ratio this mechanism is no longer operative. With $_tp_1/p_\infty = 8$, for example, comparison of Fig. 19 (lower) with Fig. 17 (lower) indicates that the minimum plug pressure is appreciably greater than the base pressure. The reason is apparent from the bottom photograph in Fig. 20 which shows that under these conditions a shock wave, produced by the base flow, traverses the primary stream. This shock wave crosses the final characteristic of the expansion fan and then intersects the plug, so that expansion is terminated before the base pressure is reached. The reasons why bleed does not influence the plug pressure distribution are, therefore, clear. At low jet pressure ratios this distribution is determined largely by the base pressure, which is practically independent of bleed (Fig. 17). At the higher jet pressure ratios bleed does increase the base pressure (Fig. 17), but the plug pressure distribution is no longer determined by the base pressure. In Fig. 19 it is important to note that, at each value of jet pressure ratio, over-expansion occurs on the plug. This over-expansion, which is negligible when $_tp_1/p_\infty = 8$. increases as the jet pressure ratio is reduced, and tends to decrease the nozzle thrust.

Fig. 21a shows the effect of bleed number on the nozzle efficiency (η_N) and the overall efficiency (η_0) at different values of jet pressure ratio. At a given jet pressure ratio, η_N depends solely on the plug pressure distribution. It is therefore independent of bleed number, but falls slightly as the jet pressure ratio is reduced, for the reasons given above. On the other hand, the overall efficiency (η_0) takes into account not only the nozzle thrust, but also the drag of the bleed system (*see* Section 4). The balance depends on both bleed number and jet pressure ratio. Thus, when $_tp_1/p_\infty = 4$, η_0 decreases with increase in H_2, because the bleed inlet momentum increases but the base pressure does not (Fig. 17). Conversely, when $_tp_1/p_\infty = 8$, η_0 increases initially with increase in H_2 because the decrease in base drag (Fig. 17) outweighs the increase in bleed inlet drag.

The thrust data are summarized in Fig. 21b. Comparing this graph with the corresponding results for $M_\infty = 0$ (Fig. 16), it will be seen that when $_tp_1/p_\infty = 6$, for example, the effect of the external stream is to reduce η_0 by $4\frac{1}{2}$ per cent. ($\eta_0 = 0{\cdot}970$ when $M_\infty = 0$ and $0{\cdot}925$ when $M_\infty = 0{\cdot}9$.) Of this reduction, 1 per cent is due to nozzle, and the remaining $3\frac{1}{2}$ per cent to the drag of the bleed system. We see also, that although base bleed increases η_0 by 0·8 per cent when $_tp_1/p_\infty = 8$, no improvement results at jet pressure ratios of 6 or less.

7.3. *Results with Model No. 1 at* $M_\infty = 2{\cdot}0$.

Fig. 22 shows the base pressure plotted against bleed number and jet pressure ratio. It is apparent that when the external stream is supersonic the base pressure is increased by bleed over the entire operating range; a result which contrasts with the subsonic behaviour described above. However, although bleed is beneficial its value is limited, and in no instance does the base pressure approach the free stream value. This limitation has serious consequences with regard to the overall thrust of the system.

Changes in flow pattern with bleed number at the design pressure ratio are clearly shown by the schlieren photographs in Fig. 23. As the bleed number increases, the free streamlines are deflected less at

the base, and the wake thickens. The external shock becomes weaker, but the strength and position of the internal shock do not change appreciably.

It follows indirectly from Fig. 22 that the ratio ${}_tp_1/p_B$ is greater than 14 (the design pressure ratio) over the whole range of the tests. In the absence of shock interference, therefore, the plug would lie entirely within an expansion fan centred at the cowl lip and the plug pressure distribution, expressed in terms of $p/{}_tp_1$, would be invariant with respect to both jet pressure ratio and bleed number. The measured distribution (Fig. 24, upper) shows that this is indeed the case provided that ${}_tp_1/p_\infty \geqslant 8$. When, however, ${}_tp_1/p_\infty < 8$, a shock wave originating in the base region intersects the plug, and the point of intersection moves upstream as the jet pressure ratio is decreased. This progression is confirmed by schlieren photographs (Fig. 25) in which the shockwave is clearly visible. Under these conditions the plug pressure distribution changes with jet pressure ratio but it is still independent of bleed number because, as mentioned above in connection with Fig. 23, the internal shock system is virtually unaffected by bleed.

It is worth noting here that the actual flow mechanism differs from that assumed in Section 2 and, in so far as the plug pressure distribution is concerned, the favourable effects of bleed predicted in that section are not realized in practice. The discrepancy arises because bleed increases the base pressure less than was anticipated. If it were possible to achieve a higher level of base pressure the argument of Section 2 would be valid.

Although shock interference prevents the plug pressure falling to excessively low values, Fig. 24 (lower) shows that the minimum static pressure on the plug is less than that of the free stream when the jet pressure ratio is less than the design value. As a result of this over-expansion, part of the plug surface experiences a drag, and the nozzle efficiency is thereby reduced. This loss in thrust increases as the jet pressure ratio falls and the point of minimum pressure moves forward along the plug.

The effect of bleed number and jet pressure ratio on the nozzle efficiency and overall efficiency are presented in Fig. 26a. Given the jet pressure ratio, η_N is determined uniquely by the plug pressure distribution. It is therefore independent of bleed number and falls with decrease in jet pressure ratio, for the reasons given above. However, bleed number has a small but significant effect on the overall efficiency. Initially η_0 increases with H_2 because the drop in base drag (Fig. 22) exceeds the rise in bleed inlet momentum. This trend is reversed if excessive bleed is used so that, at each value of jet pressure ratio, η_0 reaches a maximum when H_2 lies between 0·010 and 0·015.

Fig. 26b summarizes the thrust data. We note that η_0 with optimum bleed is approximately 1 per cent greater than η_0 without bleed over the entire range of jet pressure ratio. At the design point (${}_tp_1/p_\infty = 14$), and using optimum bleed, $\eta_0 = 0{\cdot}948$. The corresponding figure at $M_\infty = 0$ is $\eta_0 = 0{\cdot}985$ (Fig. 16) so that interference with the supersonic external stream reduces the overall efficiency by 3·7 per cent. This reduction is entirely due to the drag of the bleed system since the nozzle efficiency (η_N) is practically the same in the two cases.

7.4. *Results with Model No. 2.*

The second model, which was designed with a parabolic afterbody and no base, operates without bleed. This model was intended primarily to serve as a reference standard with which to compare the detailed results obtained with Model No. 1, and for this purpose it was considered unnecessary to analyse the overall efficiency into its components. Accordingly, neither the plug nor the afterbody were equipped with pressure points, and the investigation was restricted to measurement of the overall efficiency and visualization of the flow.

Since the two models are geometrically similar as regards the primary flow, their performance is virtually identical when the ambient conditions are static. The thrust data relating to Model No. 2 at $M_\infty = 0$ have therefore been included with the corresponding results for Model No. 1 previously presented in Fig. 16, which shows the effect of jet pressure ratio on the overall efficiency. Similar data at $M_\infty = 0{\cdot}9$ and $M_\infty = 2{\cdot}0$ are presented in Figs. 27a and b, respectively. Discussion of these results is deferred to the next Section.

Changes in flow pattern with jet pressure ratio at $M_\infty = 0{\cdot}9$ are illustrated by the schlieren photographs in Fig. 28. Fig. 29 shows similar photographs taken at $M_\infty = 2{\cdot}0$.

8. *Conclusions.*

In this experiment, the performance of two plug nozzles has been investigated. These were designed to operate at the same jet pressure ratio, but one (Model No. 1) has a cylindrical afterbody with annular base bleed, while the other (Model No. 2) has a parabolic afterbody and no base or bleed. For practical purposes the most important information obtained relates to the thrust, and our conclusions will therefore be drawn on this basis. The relevant data are summarized in Fig. 30, which compares the overall efficiency of the two models with reference to typical engine operating points. These are ${}_tp_1/p_\infty = 3$ at $M_\infty = 0$, ${}_tp_1/p_\infty = 5$ at $M_\infty = 0{\cdot}9$ and ${}_tp_1/p_\infty = 14$ at $M_\infty = 2{\cdot}0$; corresponding to the take-off, stand-off and cruising conditions respectively.

Taking into account the fixed geometry, it is immediately apparent that while the thrust at $M_\infty = 2{\cdot}0$ is of the normal order, both these plug-type nozzles are exceptionally flexible with regard to off-design performance. The overall efficiency of Model No. 2, for example, is 0·960 at the cruising condition, 0·932 at stand-off, and 0·970 at take-off. It is unlikely that this level of efficiency can be realized with either a convergent-divergent or ejector nozzle without variable geometry. Nevertheless there is still room for improvement, particularly at $M_\infty = 0{\cdot}9$.

To assess the value of base bleed we compare Model No. 1 using optimum bleed with Model No. 2 at the stand-off and cruising conditions. At the stand-off condition Model No. 1 develops maximum thrust with zero base bleed and η_0 is 1·7 per cent less than with Model No. 2. At the cruising condition bleed improves the thrust of Model No. 1 but, even so, the optimum value of η_0 is 1·2 per cent less than that of Model No. 2. On this evidence it is clear that the drawback inherent in Model No. 1, namely the high drag of its bluff base, is not eliminated by bleed, and the performance of Model No. 2 is superior at both the stand-off and cruise conditions. However, we are not in a position to generalize, and changes in the design pressure ratio, the free stream Mach number, or the geometry of the nozzle and bleed system might well qualify this conclusion. In particular, it seems likely that the effect of bleed at $M_\infty = 0{\cdot}9$ could be improved by attention to the detailed design of the bleed discharge system.

Implicit in our comparison is the assumption that the secondary flow exists solely to provide base bleed. If, however, it should prove desirable to bleed off boundary-layer air in the main engine intake, a secondary flow would necessarily be available. The choice then lies between using this air as base bleed or discharging it independently through a separate nozzle. In this context η_0 for Model No. 2 should be decreased to allow for the internal and possible external drag of this alternative secondary flow system. On this basis the performance of Model No. 1 would compare more favourably and might surpass that of Model No. 2. Further development of this argument requires specific data on the alternative means adopted to dispose of the secondary air.

It is appreciated that, in practice, the choice of a propelling nozzle is not governed entirely by considerations of thrust. Other factors, including weight, thrust reversal and silencing must be taken into account. These, however, fall outside the terms of reference of this experiment.

APPENDIX A

Definitions of Thrust and Drag.

A.1. *Nozzle Thrust.*

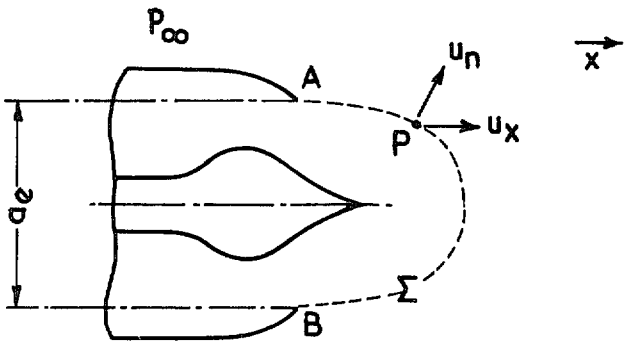

Consider, as an example, the axi-symmetric plug nozzle sketched above. Let Σ be any continuous surface through the cowl rim (AB) which does not intersect the plug. P is any point on Σ and (da) is an element of surface area enclosing P. The direction $\vec{x}$ is taken axially and downstream.

ρ is the density at P

u_x is the component of velocity at P in the direction $\vec{x}$

u_n is the component of velocity at P along the outward drawn normal to Σ

$p_x\, da$ is the component of the external force on the element (da) in direction $\vec{x}$

p_∞ is the free stream static pressure.

Then, by the momentum integral theorem, $\iint^{\Sigma} (p_x - \rho\, u_n\, u_x)\, da$ is independent of the surface of integration (Σ) and we define the nozzle thrust (S) by the equation

$$S = -\iint^{\Sigma} (p_x - \rho\, u_n\, u_x)\, da - p_\infty\, a_e. \tag{A1}$$

A.2. *Intake Drag.*

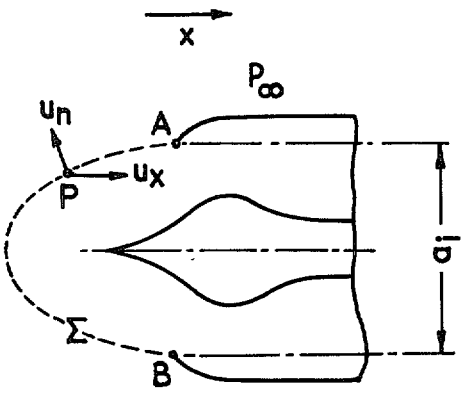

Consider the axi-symmetric centrebody intake shown, and define symbols as in Section A.1 above. Then, by the momentum integral theorem, $\iint^{\Sigma} (p_x - \rho u_n u_x)\, da$ is independent of the surface of integration (Σ) and we define the intake drag (D) by the equation

$$D = \iint^{\Sigma} (p_x - \rho\, u_n\, u_x)\, da - p_\infty\, a_i \tag{A2}$$

Although, in the interests of clarity, these two definitions have been stated for a specific type of nozzle and intake, respectively, they are of general application. Further, in the limiting case when the flow is axial and uniform in the exit (or inlet) plane, equations (A1) and (A2) reduce to the conventional definitions.

Thus, for a convergent-divergent nozzle discharging axially with uniform velocity (u_e), uniform static pressure (p_e) and uniform density (ρ_e) in the exit plane, equation (A1) reduces to

$$S = \rho_e\, u_e^2\, a_e + (p_e - p_\infty)\, a_e.$$

Similarly, for a pitot intake, assuming axial flow with uniform velocity (u_i), uniform static pressure (p_i) and uniform density (ρ_i) in the inlet plane, equation (A2) reduces to

$$D = \rho_i\, u_i^2\, a_i + (p_i - p_\infty)\, a_i.$$

A.3. *Forebody and Afterbody Drag.*

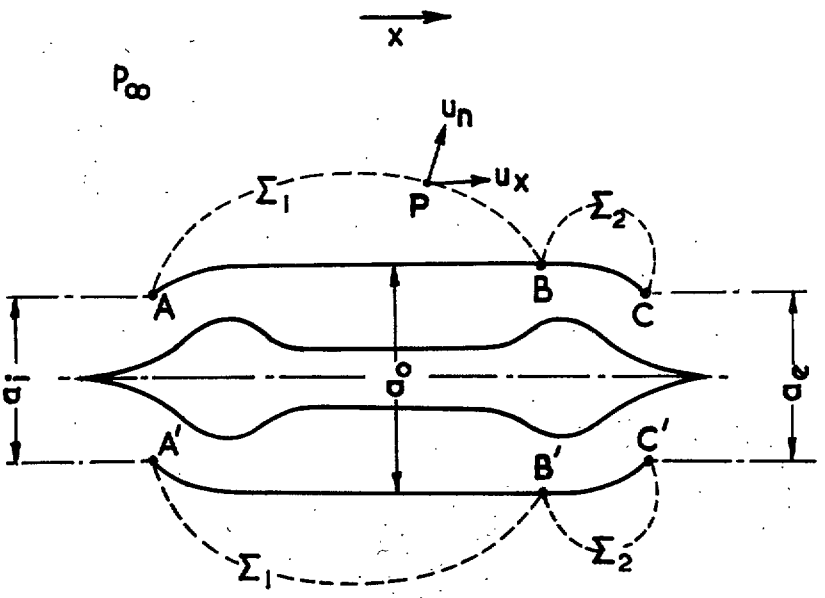

The sketch represents an axi-symmetric engine nacelle. The forebody is the external surface between planes (AA') and (BB'), and the afterbody is the external surface between planes (BB') and (CC').

Let Σ_1 be any surface enclosing the forebody, as shown, and define symbols as in Section A.1 above. Then $\iint^{\Sigma_1} (p_x - \rho\, u_n\, u_x)\, da$ is invariant with respect to Σ_1 (by the momentum integral theorem) and we define the forebody drag (D_F) by the equation

$$D_F = \iint^{\Sigma_1} (p_x - \rho\, u_n\, u_x)\, da - p_\infty\, (a_0 - a_i)\,. \tag{A3}$$

Similarly we define the afterbody drag (D_A) by the equation

$$D_A = \iint^{\Sigma_2} (p_x - \rho\, u_n\, u_x)\, da + p_\infty\, (a_0 - a_e) \tag{A4}$$

Note that if Σ_1 and Σ_2 are taken along the surface of the nacelle, u_n is zero everywhere on Σ_1 and Σ_2 so that

$$\iint^{\Sigma_1} \rho\, u_n\, u_x\, da = \iint^{\Sigma_2} \rho\, u_n\, u_x\, da = 0.$$

APPENDIX B

Analysis of Forces on Nacelle.

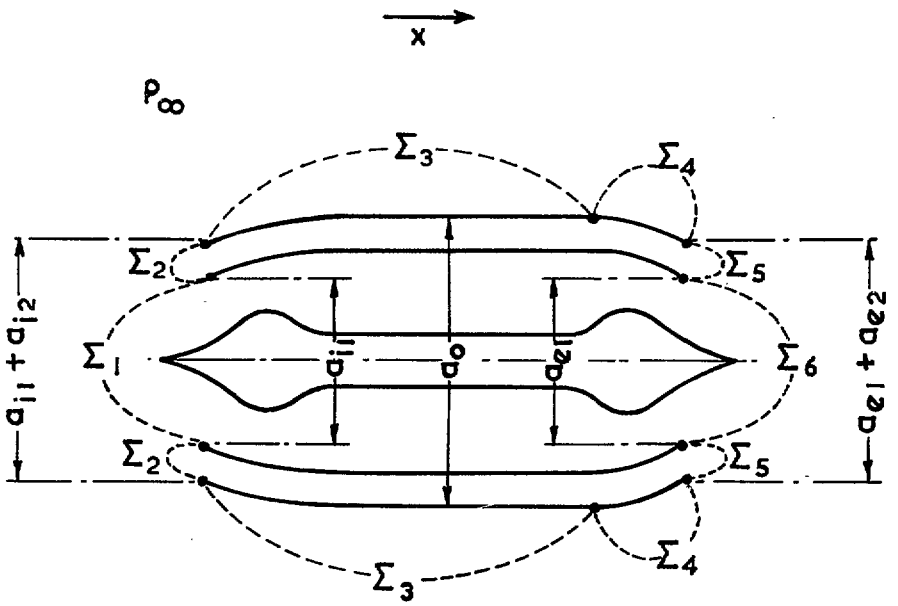

The sketch represents the general case of an axi-symmetric engine nacelle with primary and secondary flows, a forebody and an afterbody.

S_1 and S_2 are the primary and secondary nozzle thrusts, respectively.

D_1 and D_2 are the primary and secondary intake drags, respectively.

D_F is the forebody drag.

D_A is the afterbody drag.

X is the resultant axial thrust on the nacelle.

We use the notation of Appendix A and, for brevity, write

$$p_x - \rho\, u_n\, u_x = \sigma$$

at any point on the control surfaces $\Sigma_1 - \Sigma_6$.

Then the momentum integral theorem states that:—

$$-X = \iint^{\Sigma_1} \sigma\, da + \iint^{\Sigma_2} \sigma\, da + \ldots\ldots\ldots + \iint^{\Sigma_6} \sigma\, da\,. \tag{B1}$$

But, following the general definitions given in Appendix A:

$$D_1 = \iint^{\Sigma_1} \sigma\, da - p_\infty\, a_{i1} \tag{B2}$$

$$D_2 = \iint^{\Sigma_2} \sigma \, da - p_\infty \, a_{i2} \tag{B3}$$

$$D_F = \iint^{\Sigma_3} \sigma \, da - p_\infty \left[a_0 - (a_{i1} + a_{i2})\right] \tag{B4}$$

$$D_A = \iint^{\Sigma_4} \sigma \, da + p_\infty \left[a_0 - (a_{e1} + a_{e2})\right] \tag{B5}$$

$$S_2 = -\iint^{\Sigma_5} \sigma \, da - p_\infty \, a_{e2} \tag{B6}$$

$$S_1 = -\iint^{\Sigma_6} \sigma \, da - p_\infty \, a_{e1} \, . \tag{B7}$$

Substituting equations (B2) to (B7) in (B1) gives

$$X = (S_1 + S_2) - (D_1 + D_2 + D_F + D_A) \, . \tag{B8}$$

Now the primary object of the experimental work is to compare two engine installations of the form shown below.

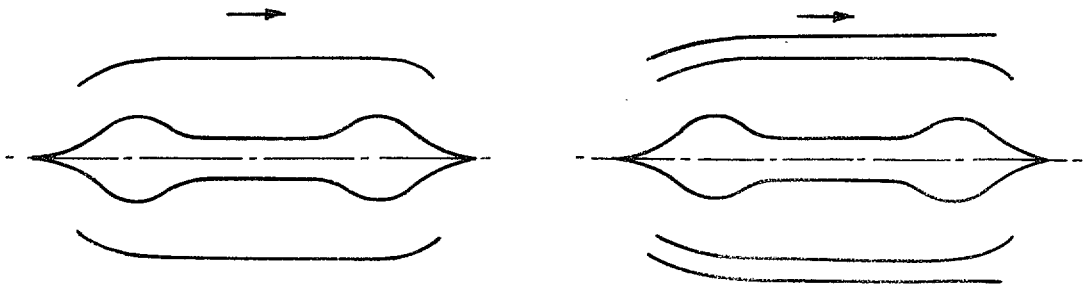

In the left-hand diagram, corresponding to Model No. 2, a given turbo-jet engine and intake, operating at given conditions, discharge through a simple plug nozzle without secondary flow.

In the right-hand diagram, corresponding to Model No. 1, the same engine and intake, operating at the same conditions, discharge through a plug nozzle with a cylindrical afterbody and secondary flow (base bleed).

On this basis D_1 will be the same for the two configurations and the difference in D_F will be of the second order only. If then, we define

$$Y = (S_1 + S_2) - (D_2 + D_A) \tag{B9}$$

equation (B8) shows that (Y) is a direct measure of (X), the resultant axial thrust on the nacelle.

We note also that for Model No. 1 $D_A = 0$ so that

$$Y = S_1 + S_2 - D_2 \tag{B10}$$

and for Model No. 2 $D_2 = S_2 = 0$,

so that

$$Y = S_1 - D_A \, . \tag{B11}$$

APPENDIX C

Analysis of Forces on Plug Nozzle.

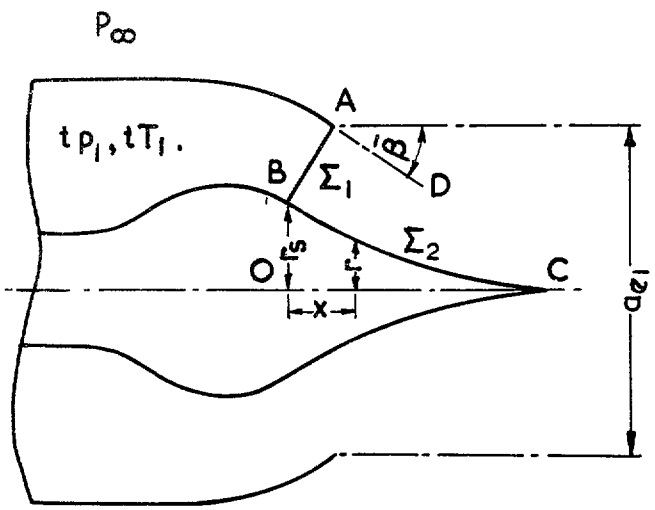

In the axi-symmetric plug nozzle shown above, AD represents the tangent at A to the internal surface of the cowl. AB is taken perpendicular to AD and it is assumed that at any point on AB the flow is sonic and normal to AB, so that B is the sonic point on the plug. Σ is a control surface through the cowl rim which is divided into two parts, Σ_1 which coincides with AB, and Σ_2 which coincides with the plug surface between B and C.

Then, using the notation and definitions of Appendix A (Section 1), the nozzle thrust (S_1) is given by:

$$S_1 = -\iint^{\Sigma_1} (p_x - \rho\, u_n\, u_x)\, da - \iint^{\Sigma_2} (p_x - \rho\, u_n\, u_x)\, da - p_\infty\, a_{e1}\,. \tag{C1}$$

Assume that, in the jet pipe, the stagnation pressure ($_tp_1$) and the stagnation temperature ($_tT_1$) are uniform across the section, and expansion is isentropic up to the throat (AB). Then, on AB, u_{th}, p_{th} and ρ_{th} are uniform and, by hypothesis, $M_{th} = 1$. Let a_{th} denote the throat area (normal to the flow).

Then on Σ_1

$$p_x = -p_{th} \cos \overline{\beta}$$

$$U_n = u_{th}$$

and

$$u_x = u_{th} \cos \overline{\beta}$$

so that

$$\iint^{\Sigma_1} (p_x - \rho\, u_n\, u_x)\, da = -\cos\bar{\beta}\,(p_{th} + \rho_{th}\, u_{th}^2)\, a_{th}$$

which reduces to

$$\frac{1}{a_{th}\, p_\infty} \iint^{\Sigma_1} (p_x - \rho\, u_n\, u_x)\, da = -(\gamma+1)\left(\frac{\gamma+1}{2}\right)^{\frac{\gamma}{1-\gamma}} \cos\bar{\beta}\,\frac{p_1}{p_\infty}. \tag{C2}$$

Now, at any point on Σ_2, $u_n = 0$, and if we neglect skin friction

$$p_x\, da = -2\pi\, pr\, dr$$

so that

$$\iint^{\Sigma_2} (p_x - \rho\, u_n\, u_x)\, da = -2\pi \int_0^{r_s} pr\, dr\,.$$

Hence, defining

$$\lambda = p/p_\infty$$

$$\mu = r/r_s$$

and noting that, by geometry, $a_{e1} = \pi\, r_s^2 + a_{th} \cos\bar{\beta}$

we find that

$$\frac{1}{a_{th}\, p_\infty} \iint^{\Sigma_2} (p_x - \rho\, u_n\, u_x)\, da = -2\left(\frac{a_{e1}}{a_{th}} - \cos\bar{\beta}\right) \int_0^1 \lambda\, \mu\, d\,\mu\,. \tag{C3}$$

Finally, substituting equations C2 and C3 in equation C1 we get

$$\frac{S_1}{a_{th}\, p_\infty} = (\gamma+1)\left(\frac{\gamma+1}{2}\right)^{\frac{\gamma}{1-\gamma}} \cos\bar{\beta}\,\frac{p_1}{p_\infty} + 2\left(\frac{a_{e1}}{a_{th}} - \cos\bar{\beta}\right) \int_0^1 \lambda\, \mu\, d\,\mu - \frac{a_{e1}}{a_{th}}. \tag{C4}$$

This equation (C4) expresses the thrust in terms of the integrated plug pressure distribution for a nozzle of given geometry operating under given conditions.

LIST OF SYMBOLS

The notation is shown, in part, in Fig. 5. Definitions of thrust and drag are given in Appendix A and efficiencies are defined in Section 4.

1. *Suffixes, etc.*

$( )_1$	denotes the primary flow
$( )_2$	denotes the secondary flow
$( )_i$	denotes the inlet plane
$( )_0$	denotes the maximum cross section (when applied to an area)
$( )_{th}$	denotes the nozzle throat
$( )_e$	denotes the exit plane
$( )_B$	denotes the base
$( )_\infty$	denotes the free stream
$\overline{( )}$	denotes the design condition
$( )^*$	denotes isentropic conditions
${}_t( )$	denotes stagnation conditions

Suffixes are combined where appropriate. Thus a_{e1} is the exit area of the primary flow (*see* Fig. 5).

2. *Flow parameters.*

M	Mach number
u	Velocity
ρ	Density
p	Static pressure
T	Static temperature
Q	Rate of mass flow
β	Prandtl-Meyer angle
μ	Mach angle
γ	Ratio of specific heats
R	Gas constant
H	Bleed number

$$H_2 = \sqrt{\frac{R}{\gamma}} \frac{Q_2 \sqrt{{}_tT_\infty}}{a_{e2}\, {}_tp_\infty}$$

In the present experiment $H_2 = 0{\cdot}259 \dfrac{{}_tp_1}{p_\infty} \dfrac{Q_2}{Q_1}$ when $M_\infty = 0{\cdot}9$

$$H_2 = 0{\cdot}056 \frac{{}_tp_1}{p_\infty} \frac{Q_2}{Q_1} \text{ when } M_\infty = 2{\cdot}0$$

3. *Geometrical Parameters.*

a	Area
r	Radius
d	Diameter
x	Axial distance from assumed sonic point on plug
l	Length of plug from assumed sonic point to vertex
L	Axial distance from inlet plane of wind tunnel nozzle to base of model
$\overline{\beta}$	Angle between internal tangent to cowl at exit and axis

4. *Force Parameters.*

S	Thrust
D	Drag
η	Efficiency

5. *Nomenclature.*

${}_tp_1/p_\infty$	is called the jet pressure ratio
a_{e1}/a_0	is called the nozzle area ratio

REFERENCES

No.	*Author*	*Title, etc.*
1	J. Reid	An experiment on aerodynamic nozzles at $M = 2$. A.R.C. R. & M. 3382. November 1962.
2	H. G. Krull and W. T. Beale ..	Effect of plug design on performance characteristics of convergent-plug exhaust nozzles. NACA Research Memo E54 H05. October 1954.
3	H. G. Krull and W. T. Beale ..	Effect of outer-shell design on performance characteristics of convergent-plug exhaust nozzles. NACA Research Memo E54 K22. April 1955.
4	H. G. Krull and W. T. Beale ..	Comparison of two methods of modulating the throat area of convergent plug nozzles. NACA Research Memo E54 L08. May 1955.
5	H. G. Krull, W. T. Beale and R. F. Schmiedlin	Effect of several design variables on internal performance of cinvergent-plug exhaust nozzles. NACA Research Memo E56 G20. October 1956.
6	A. S. Valerino, R. F. Zappa and K. L. Abdalla	Effects of external stream on the performance of isentropic plug-type nozzles at Mach number of 2·0, 1·8 and 1·5. NASA Memo 2–17–59E. March 1959.
7	J. Reid and R. C. Hastings ..	The effect of a central jet on the base pressure of a cylindrical afterbody in a supersonic stream. A.R.C. R. & M. No. 3224. December 1959.
8	J. Reid and R. C. Hastings ..	Experiments on the axi-symmetric flow over afterbodies and bases at $M = 2{\cdot}0$. A.R.C. 21707. October 1959.
9	A. G. Kurn	A base pressure investigation, at transonic speeds, on an afterbody containing four sonic nozzles and a cylindrical afterbody containing a central sonic nozzle. A.R.C. 24932. February 1963.
10	J. M. Cubbage, Jr.	Jet effects on base and afterbody pressures of a cylindrical afterbody at transonic speeds. NACA Research Memo L56 C21. May 1956.

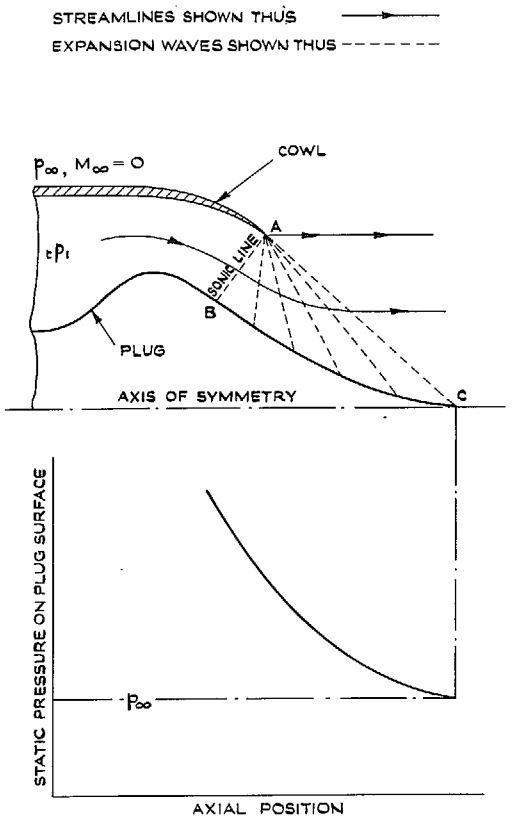

FIG. 1. Axi-symmetric plug nozzle with no external flow. Jet pressure ratio equals design pressure ratio.

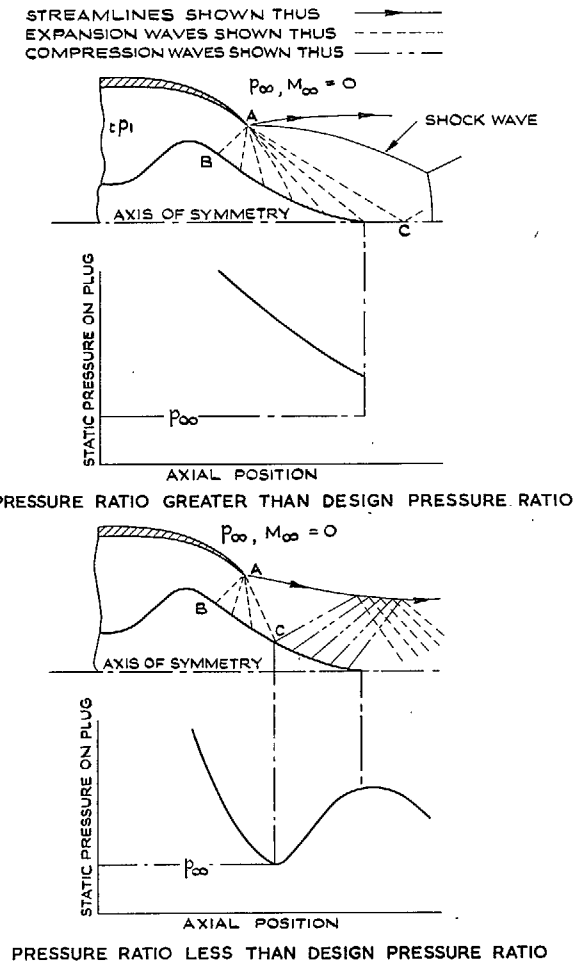

FIG. 2a & b. Axi-symmetric plug nozzle with no external flow.

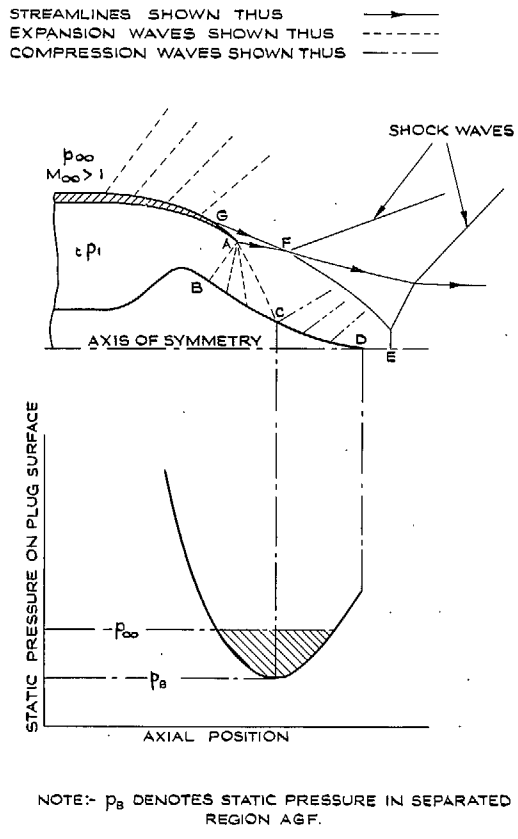

NOTE:- p_B DENOTES STATIC PRESSURE IN SEPARATED REGION AGF.

FIG. 3. Axi-symmetric plug nozzle with supersonic external flow. Jet pressure ratio less than design pressure ratio.

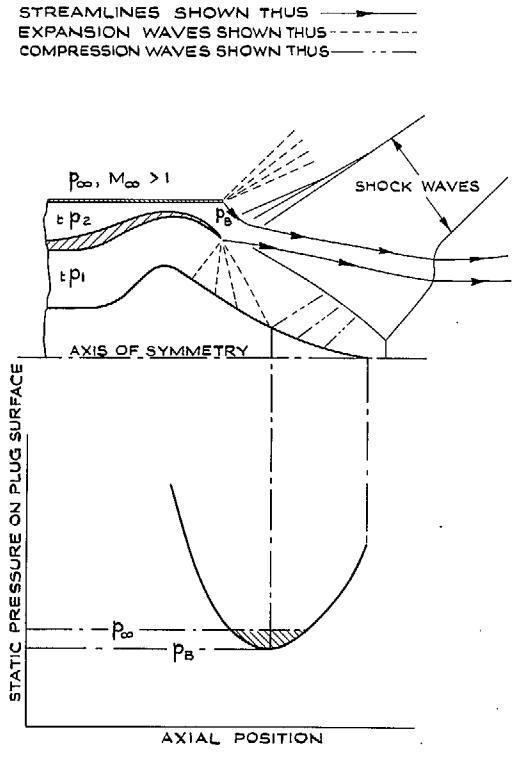

FIG. 4. Axi-symmetric plug nozzle with base bleed. Supersonic external flow. Jet pressure ratio less than design pressure ratio.

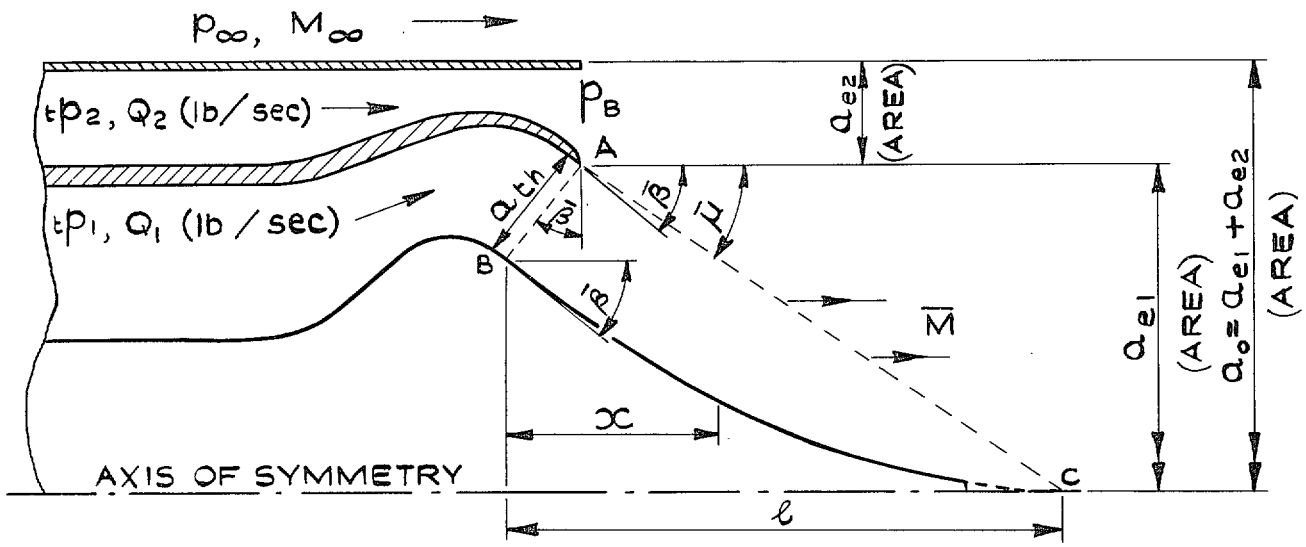

(a) PLUG NOZZLE WITH BASE BLEED (MODEL No.1)

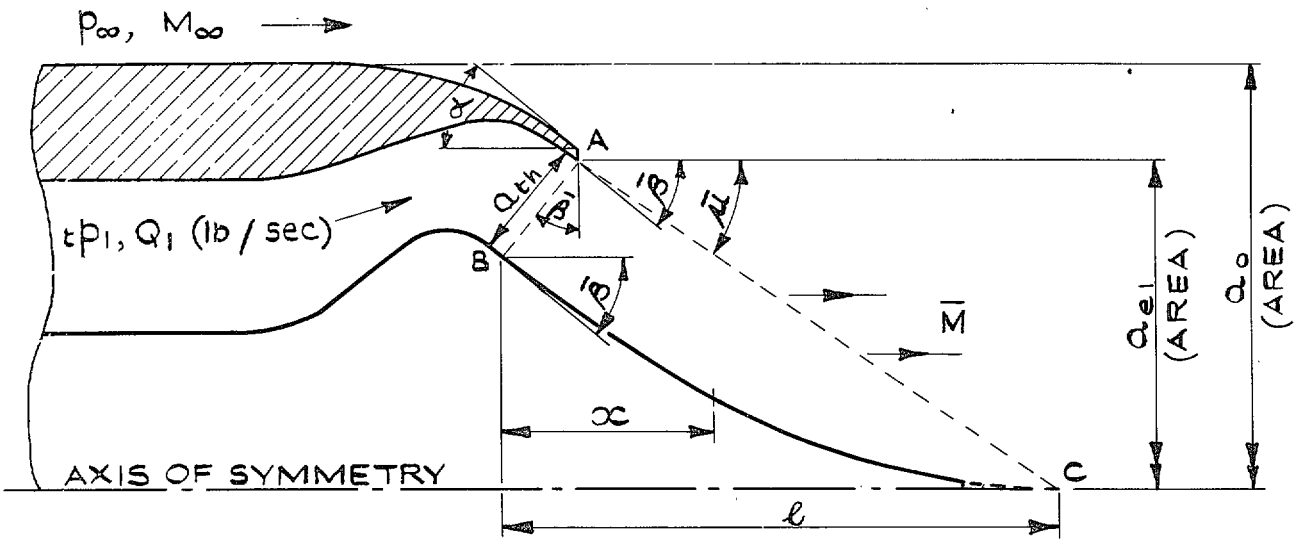

(b) SIMPLE PLUG NOZZLE (MODEL No. 2)

NOTE:- (BOTH FIGURES)

$\left(\overline{tp_1/p_\infty}\right)$ ≡ DESIGN PRESSURE RATIO

$\bar{M}$ ≡ DESIGN MACH NUMBER

$\bar{\beta}$ ≡ PRANDTL - MEYER ANGLE CORRESPONDING TO $\bar{M}$

$\bar{\mu}$ ≡ MACH ANGLE CORRESPONDING TO $\bar{M}$

"A B" IS SONIC LINE

FIG. 5a & b. Schematic diagram showing notation.

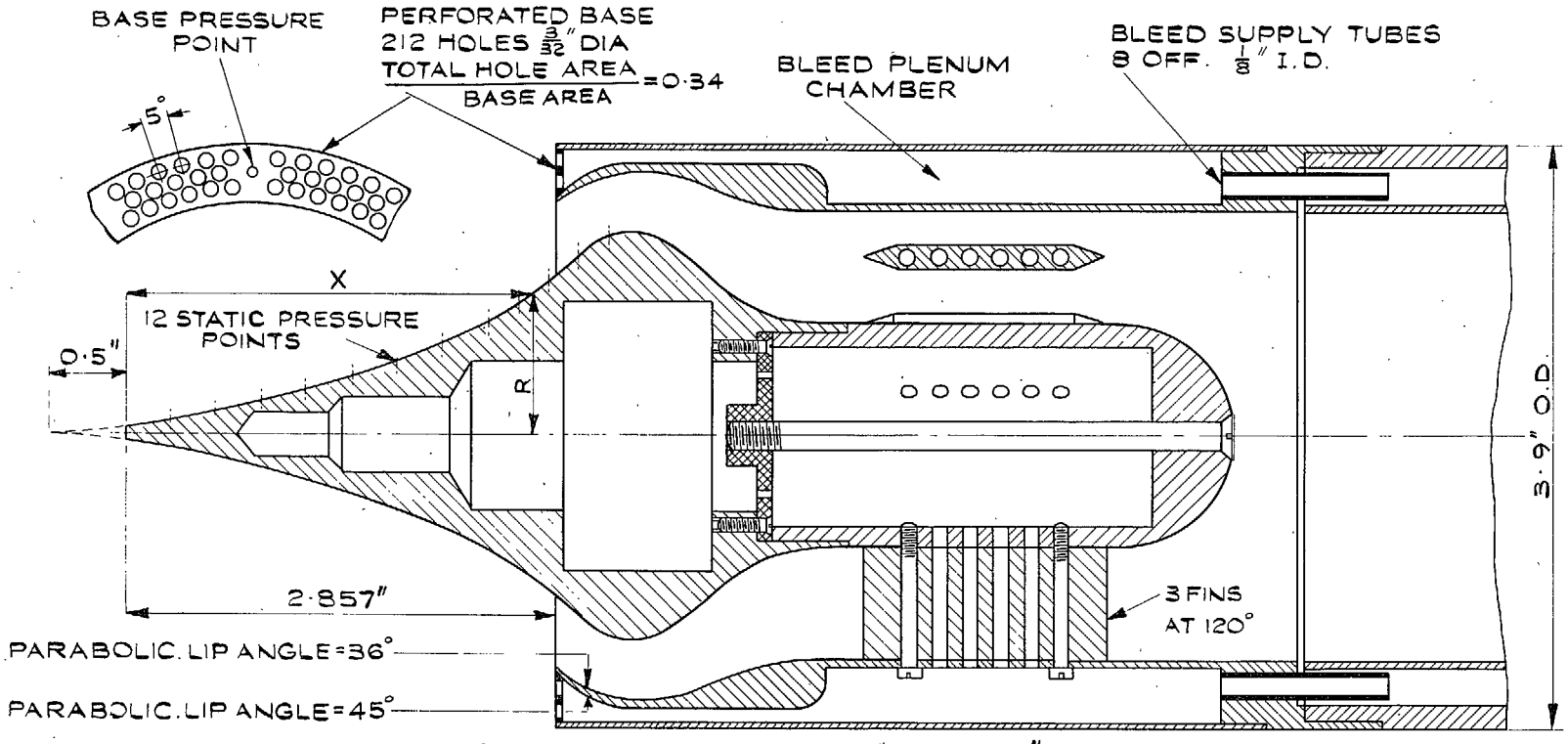

PLUG CO-ORDINATES.. (SONIC POINT AT X = 3·075" R = 1·264")

X"	0·0	0·1	0·3	0·5	0·7	0·9	1·1	1·3	1·5	1·7	1·9	2·1	2·3	2·5	2·7	2·9	3·0	3·1
R"	0·033	0·048	0·085	0·127	0·172	0·220	0·271	0·327	0·387	0·453	0·526	0·607	0·702	0·810	0·940	1·108	1·203	1·281

PLUG PRESSURE POINTS

No	1	2	3	4	5	6	7	8	9	10	11	12
X"	3·2	3·0	2·8	2·6	2·4	2·1	1·8	1·5	1·2	0·9	0·6	0·3

FIG. 6. Model No. 1. $\overline{{}_{t}p_1/p_\infty} = 14{\cdot}0$. $a_{e1}/a_0 = 0{\cdot}64$.

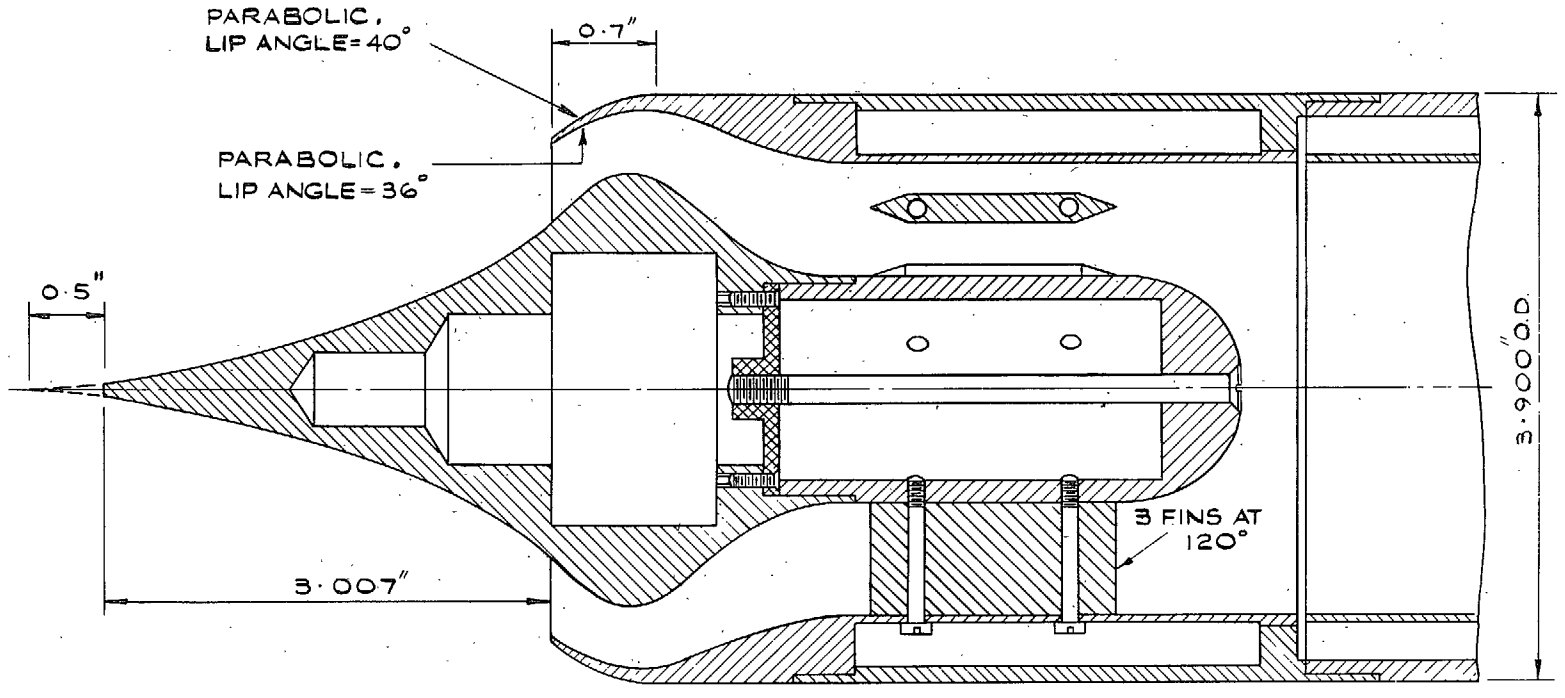

FIG. 7. Model No. 2 $\overline{{}_{t}p_1/p_\infty} = 14{\cdot}0$. $a_{e1}/a_0 = 0{\cdot}70$.

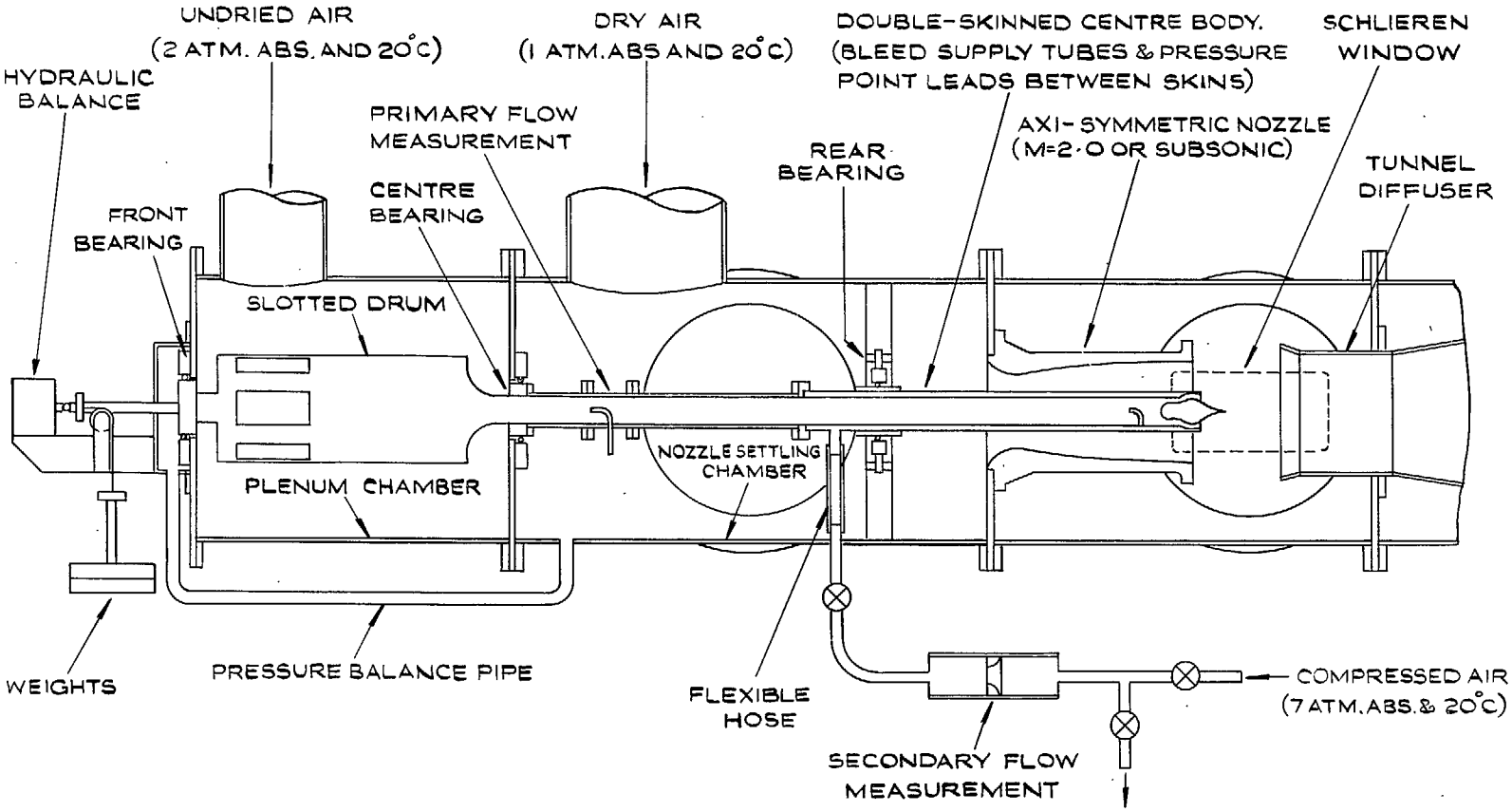

FIG. 8. The jet interference tunnel (No. 16).

NOTE:-

THE CENTRE BODY EXTENDS TO L=28 in

M_∞ IS REFERRED TO THE AMBIENT STATIC DISCHARGE PRESSURE

LEGEND

FULL LINE DENOTES MACH NUMBER ON CENTRE BODY

DOTTED LINE DENOTES MACH NUMBER ON NOZZLE WALL

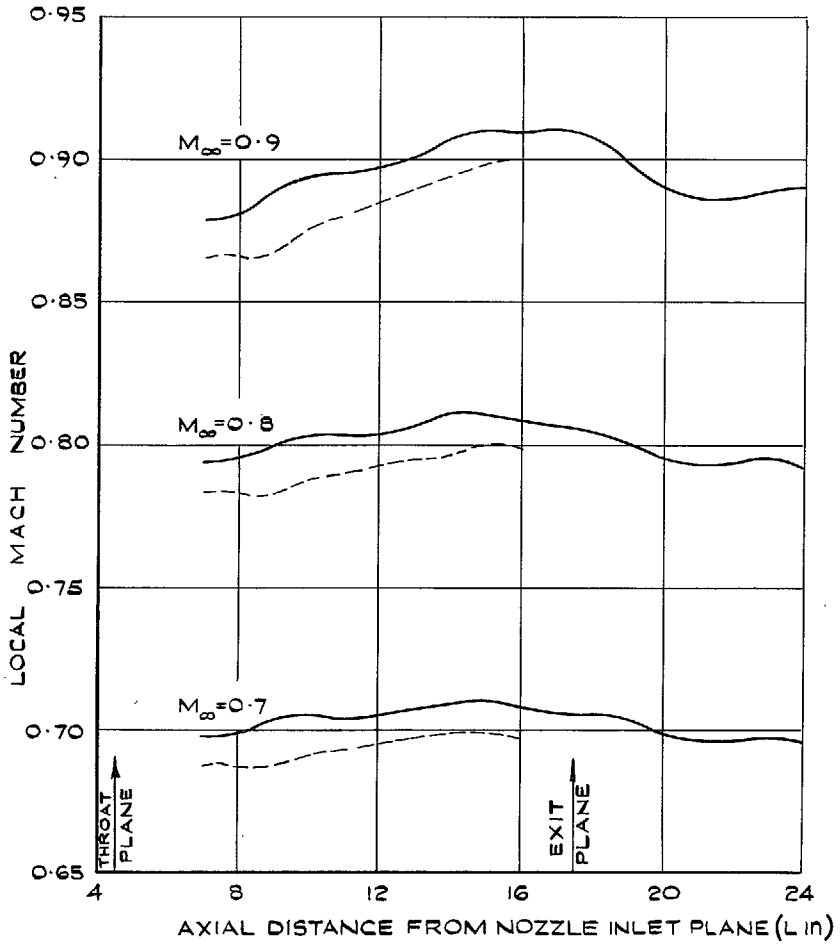

FIG. 9. Calibration of subsonic tunnel nozzle.

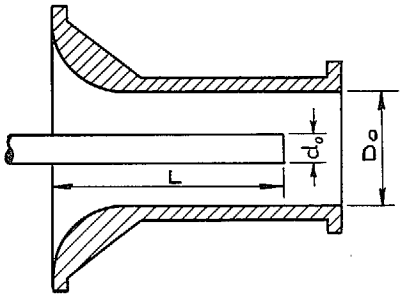

SOURCE OF DATA	TUNNEL TYPE	TUNNEL DIMENSIONS	d_o (in)	L (in)	BLOCKAGE (%)	SYMBOL
PRESENT TESTS	OPEN JET NOT SLOTTED	10 in DIA	3·9	17·5	15·2	—⊙—
PRESENT TESTS	OPEN JET NOT SLOTTED	10 in DIA	3·9	23·5	15·2	—×—
REF. 9	CLOSED JET SLOTTED	24 in x 18 in	2·75	—	1·4	---⊡---
REF.10	CLOSED JET SLOTTED	12 in x 8·5 in	2·0	—	3·1	-—◇—-

N.B. BLOCKAGE $(\%) = 100 \times \left(\frac{d_o}{D_o}\right)^2$

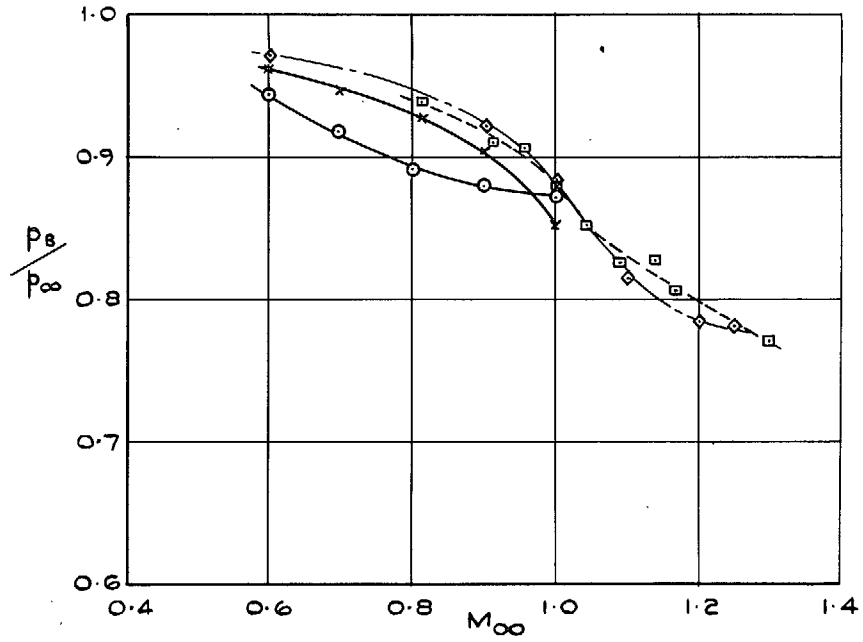

FIG. 10. Comparison of transonic base pressure measurements in different wind tunnels.

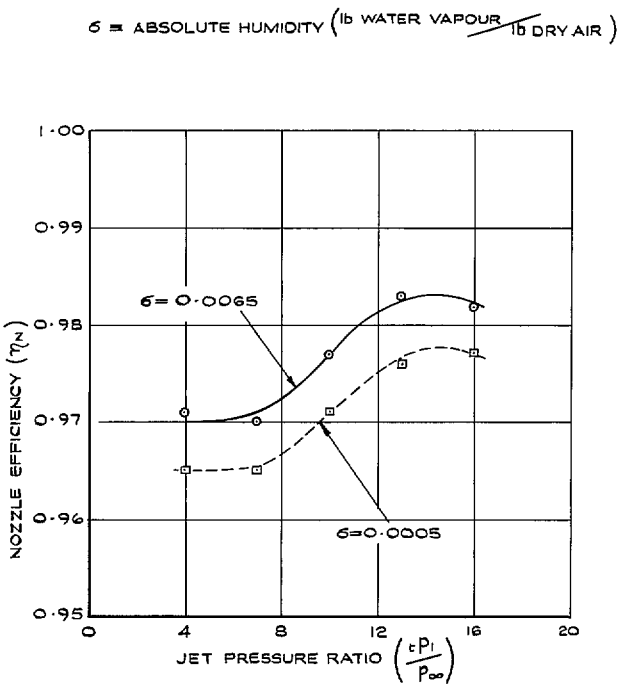

FIG. 11. The effect of water vapour on the nozzle efficiency. Model No. 2 $M_\infty = 0$.

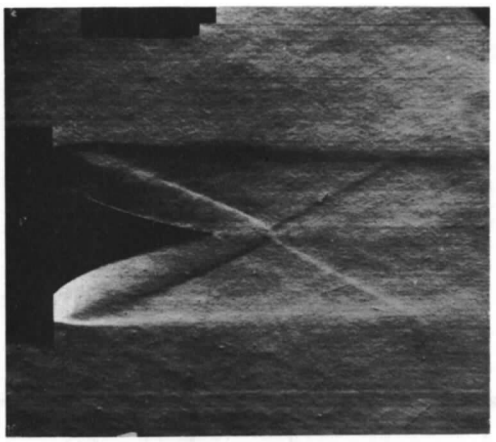

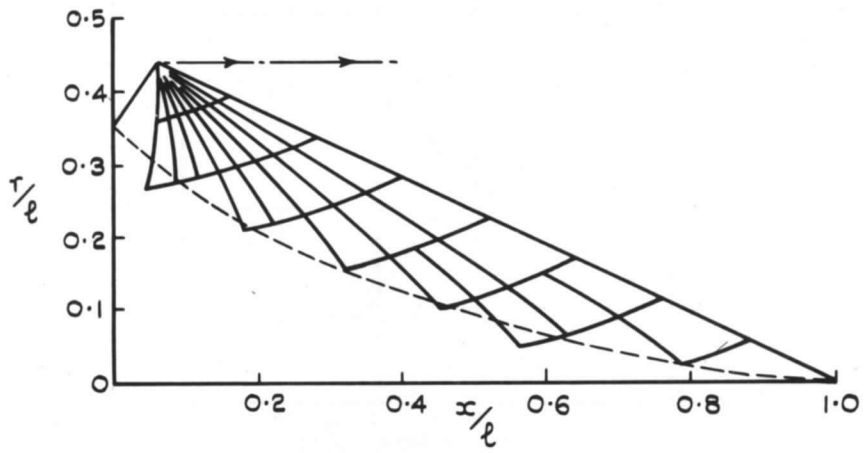

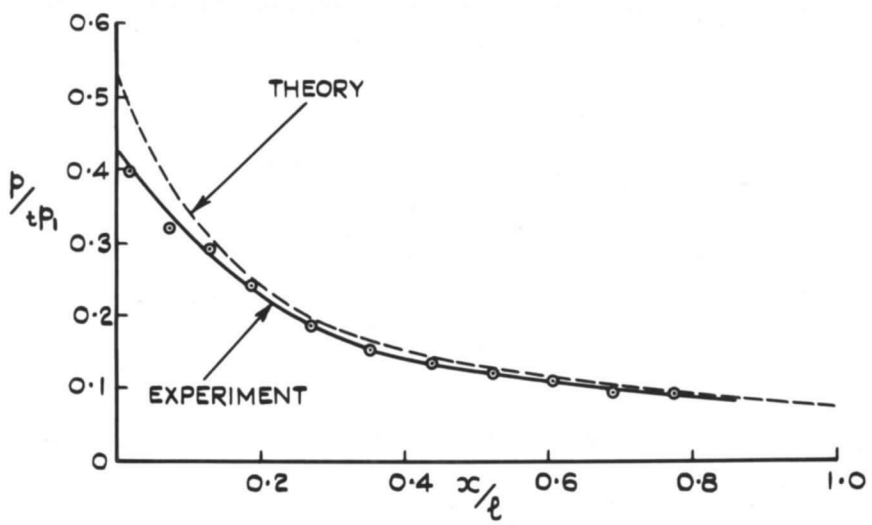

FIG. 12. The flow field. Comparison of theory with experiment.

Model No. 1. $M_\infty = 0.$ $\frac{tp_1}{p_\infty} = 14{\cdot}0.$

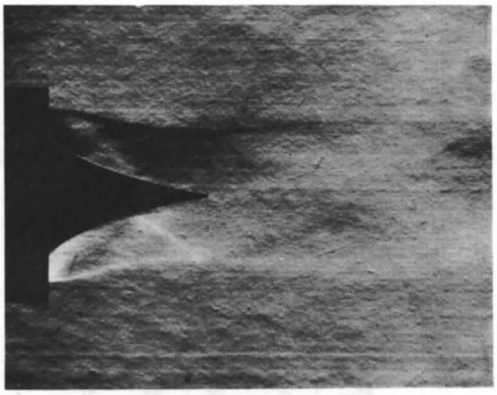

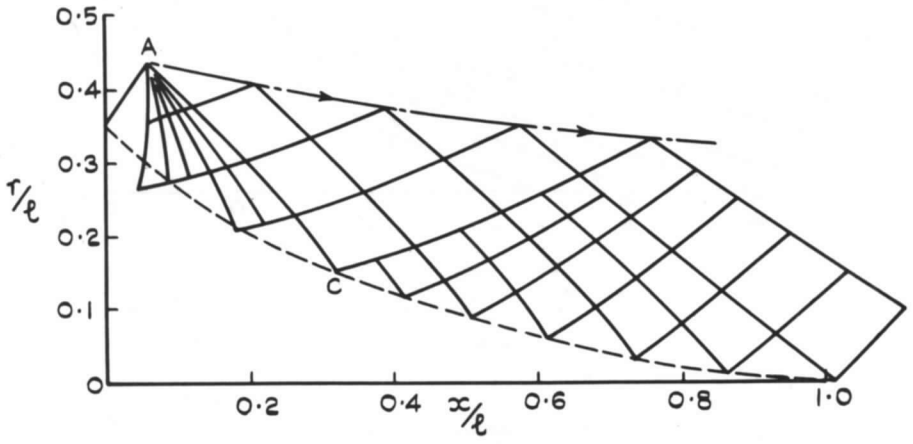

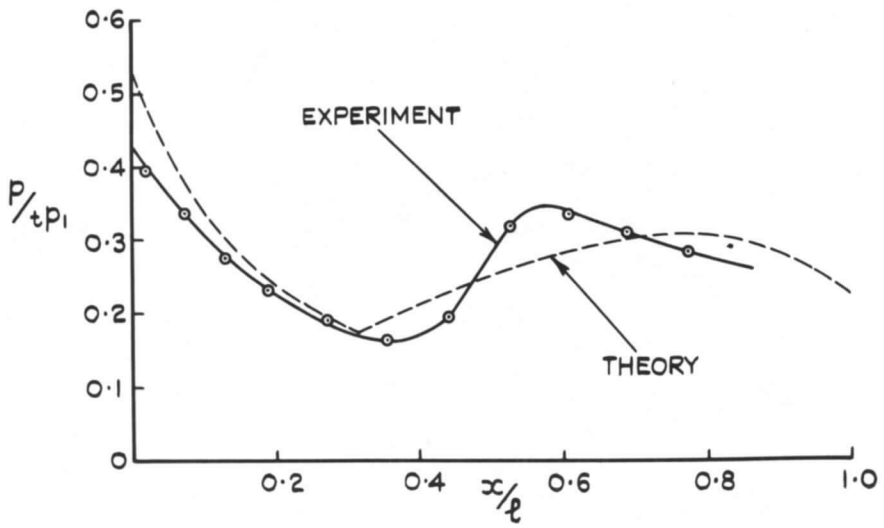

FIG. 13. The flow field. Comparison of theory with experiment.

Model No. 1. $M_\infty = 0$. $\frac{{}_tp_1}{p_\infty} = 7{\cdot}0$.

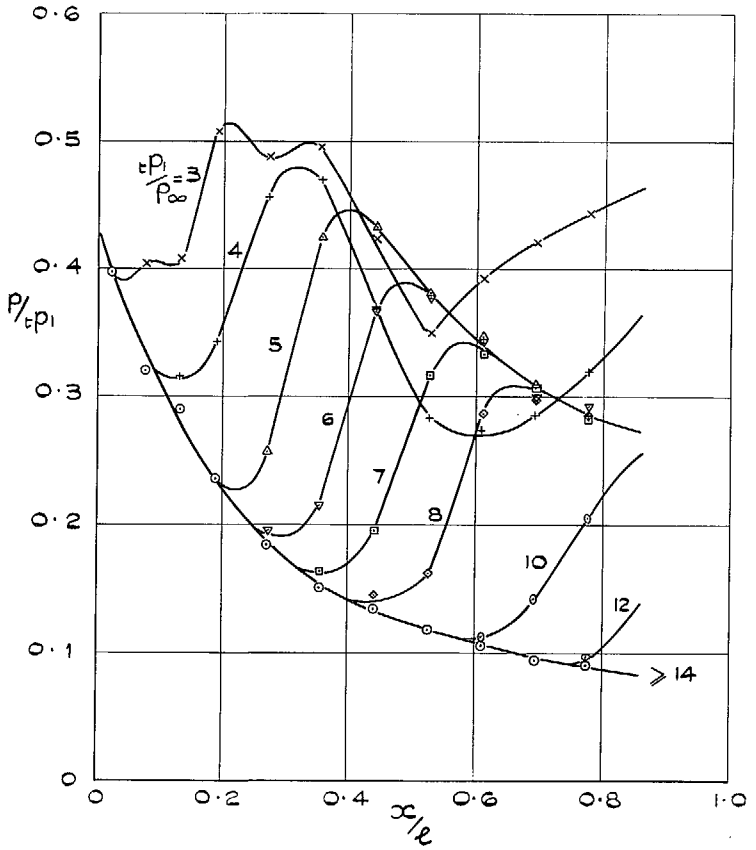

FIG. 14a. The effect of jet pressure ratio on the plug pressure distribution. Model No. 1. $M_\infty = 0$.

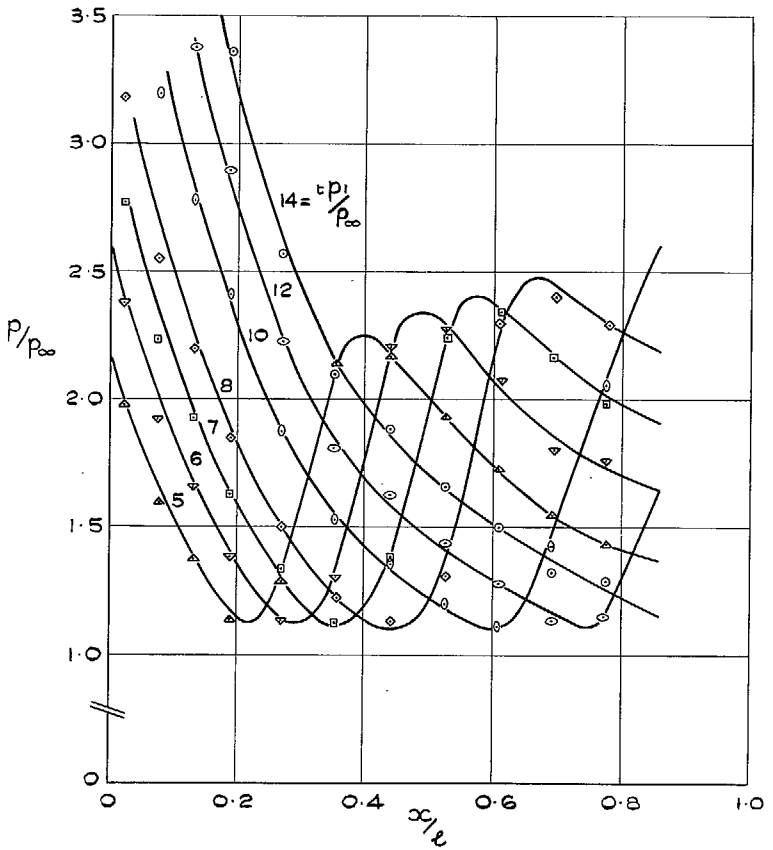

FIG. 14b. The effect of jet pressure ratio on the plug pressure distribution. Model No. 1. $M_\infty = 0$.

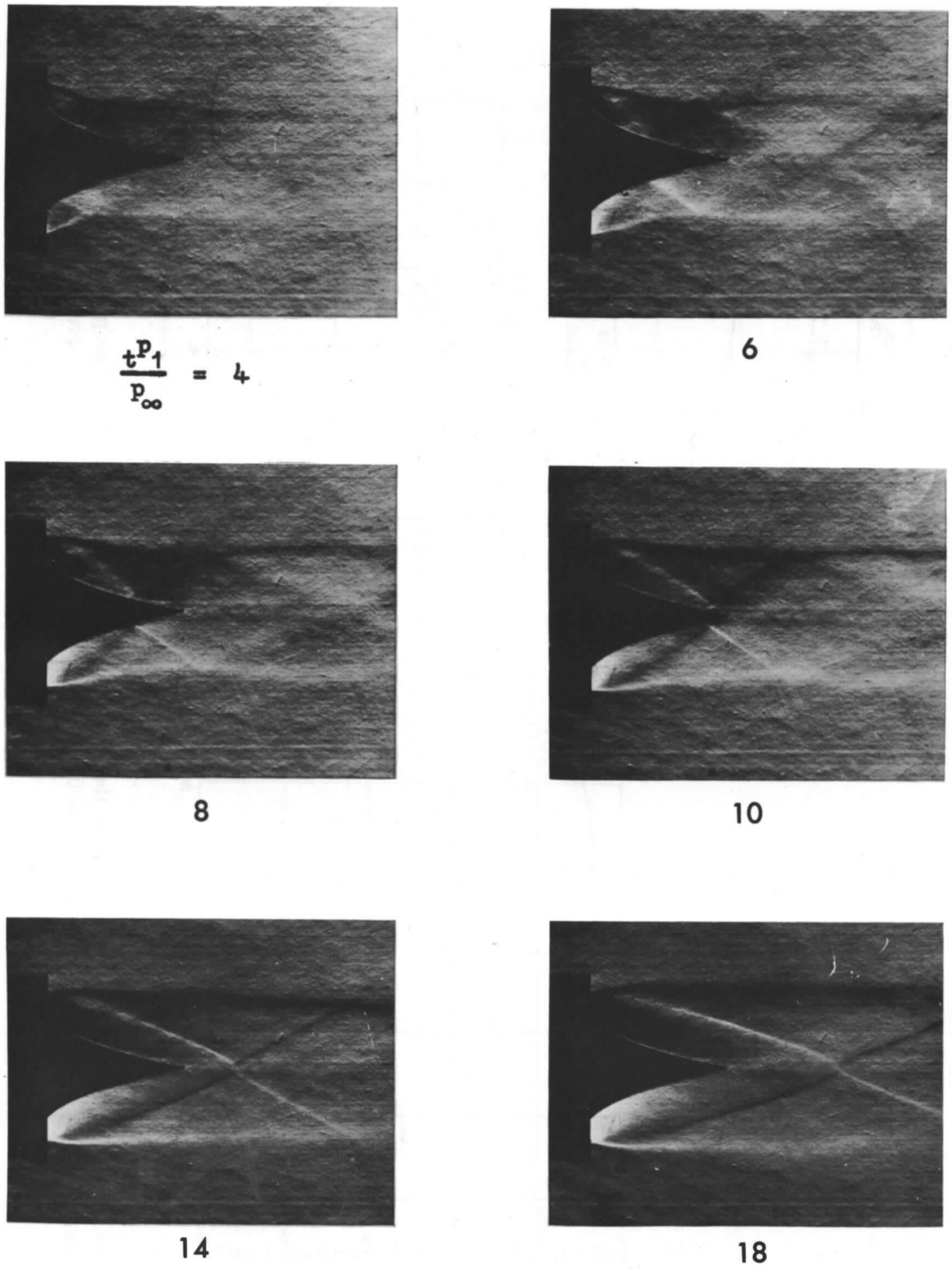

FIG. 15. Schlieren photographs showing the effect of jet pressure ratio on the flow field. Model No. 1. $M_\infty = 0$.

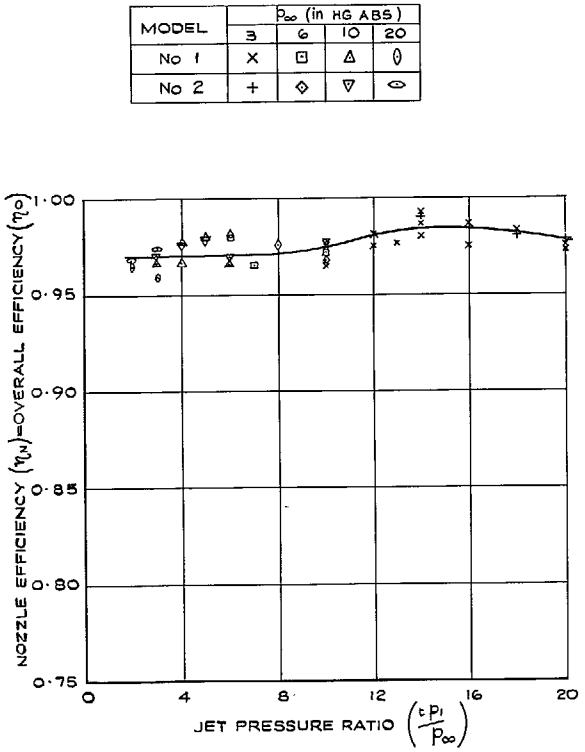

FIG. 16. The effect of jet pressure ratio on the nozzle efficiency. Models No. 1 & 2. $M_\infty = 0$.

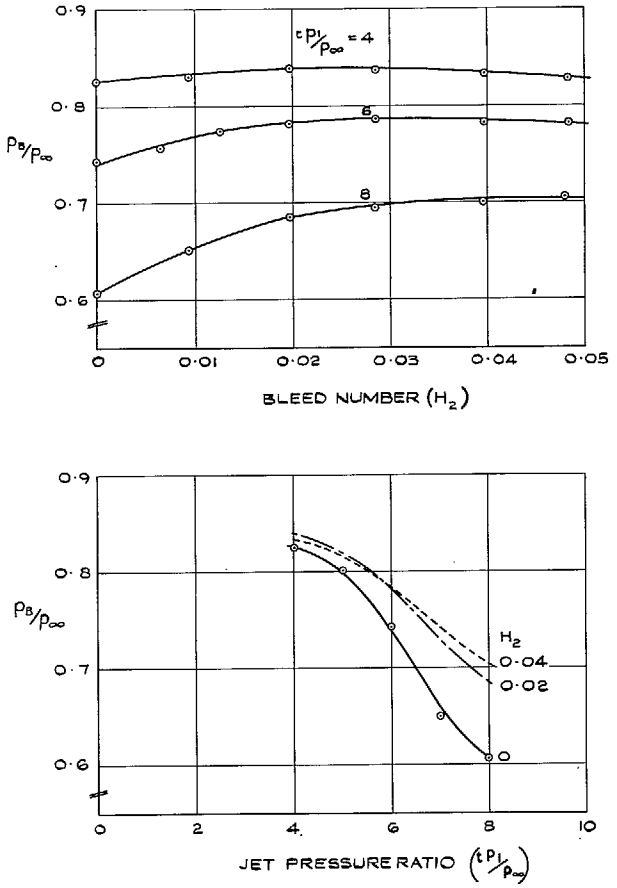

FIG. 17. The effect of jet pressure ratio and bleed number on the base pressure. Model No. 1. $M_\infty = 0{\cdot}9$.

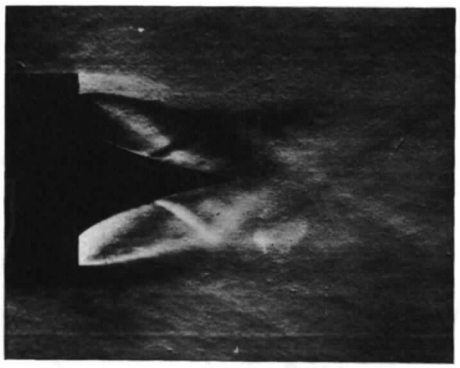

$H_2=0$

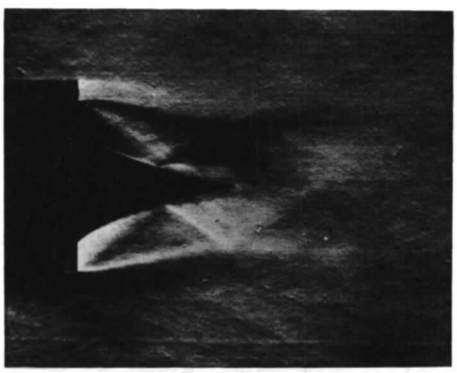

0.025

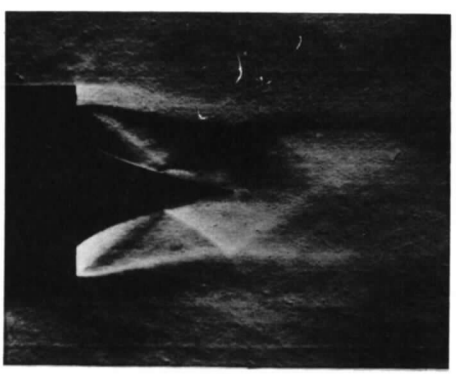

0.050

FIG. 18. Schlieren photographs showing the effect of bleed number on the flow field.

Model No. 1. $M_\infty = 0{\cdot}9 \frac{{}_tp_1}{p_\infty} = 6.$

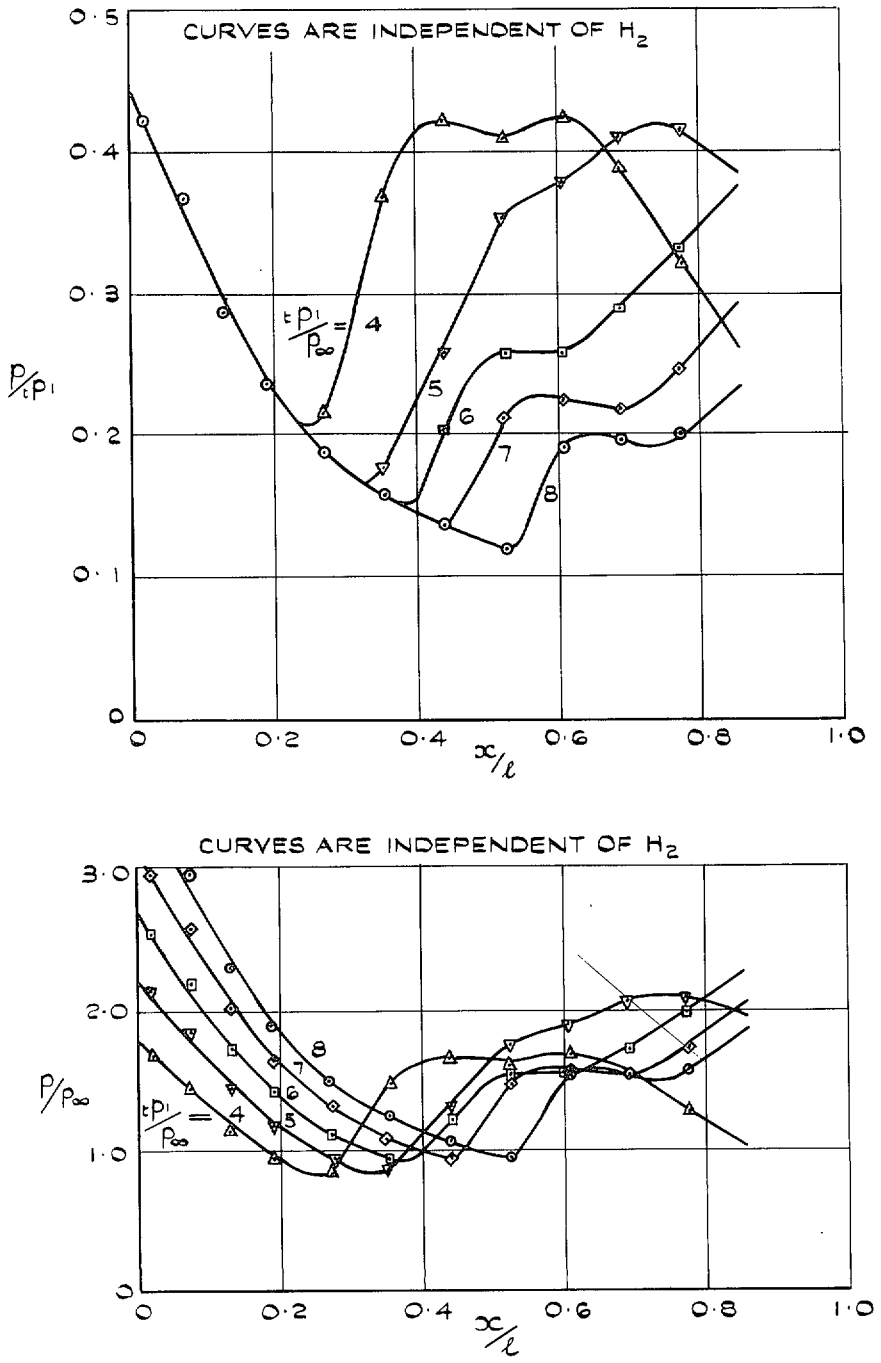

FIG. 19. The effect of jet pressure ratio on the plug pressure distribution. Model No. 1. $M_\infty = 0{\cdot}9$.

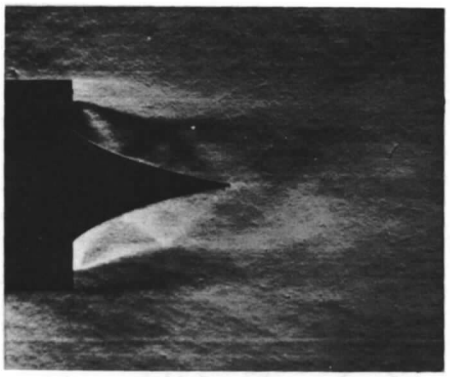

$\frac{t^{p_1}}{p_\infty} = 4$

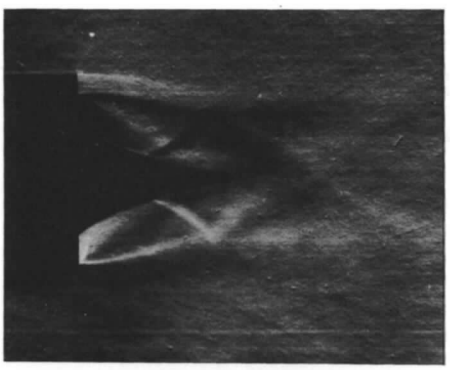

6

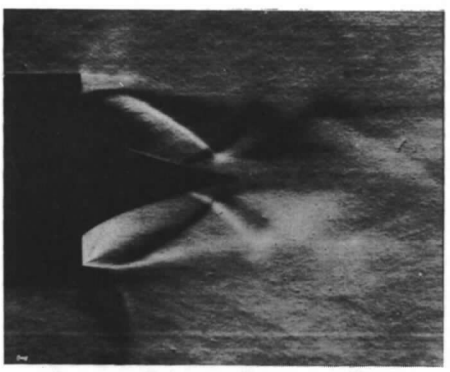

8

FIG. 20. Schlieren photographs showing the effect of jet pressure ratio on the flow field.
Model No. 1. $M_\infty = 0{\cdot}9$. $H_2 = 0$.

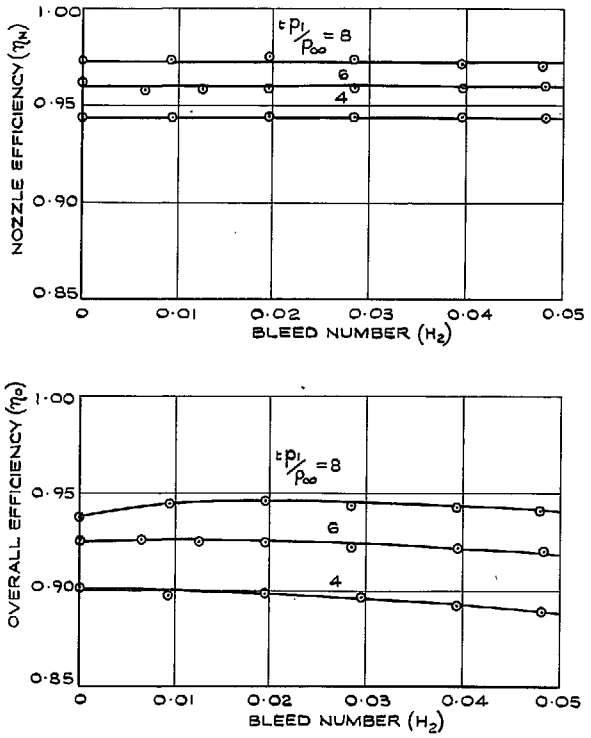

FIG. 21a. The effect of jet pressure ratio and bleed number on the nozzle efficiency and overall efficiency. Model No. 1. $M_\infty = 0{\cdot}9$.

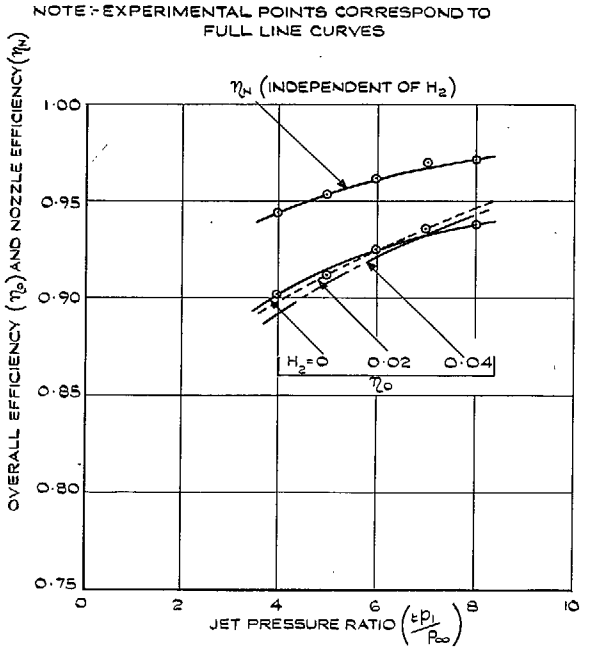

FIG. 21b. The effect of jet pressure ratio and bleed number on the nozzle efficiency and overall efficiency. Model No. 1. $M_\infty = 0{\cdot}9$.

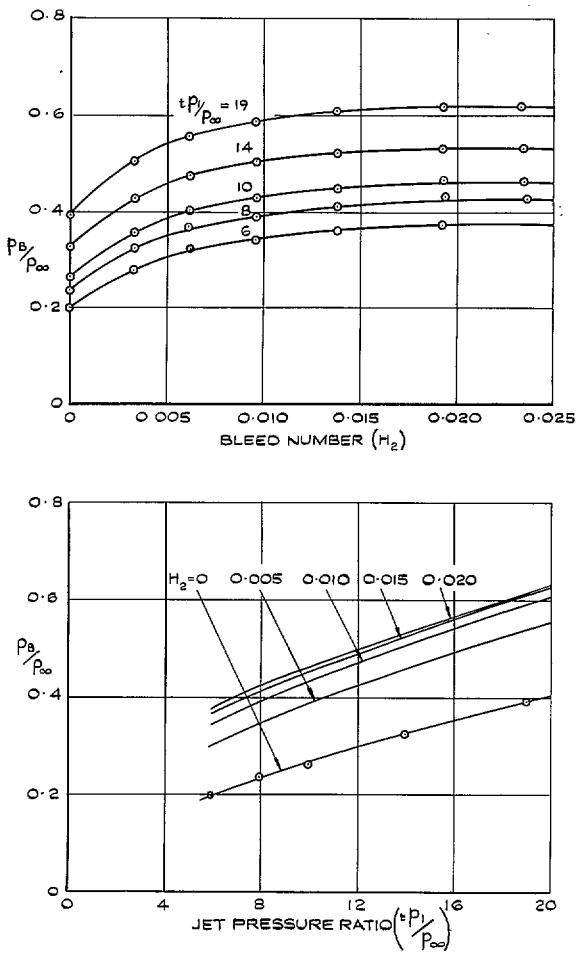

FIG. 22. The effect of jet pressure ratio and bleed number on the base pressure. Model No. 1. $M_\infty = 2{\cdot}0$.

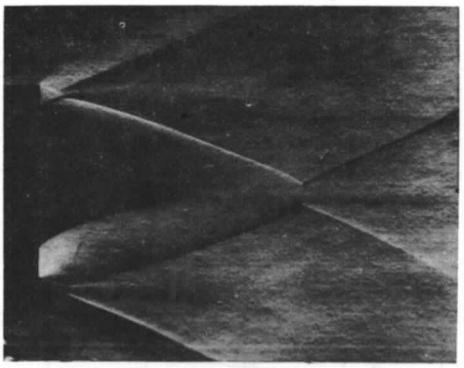

$H_2=0$

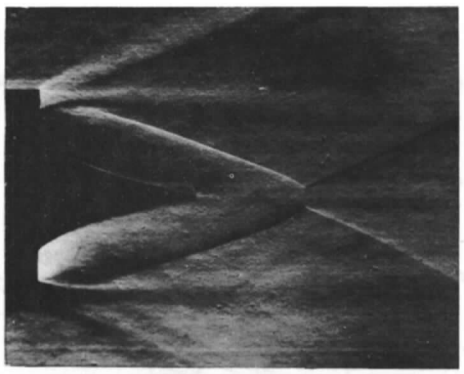

0.014

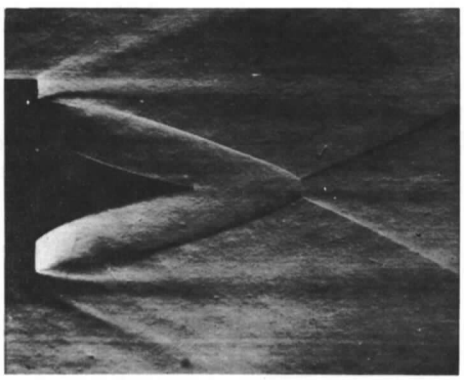

0.024

FIG. 23. Schlieren photographs showing the effect of bleed number on the flow field.

Model No. 1. $M_\infty = 2{\cdot}0$. $\frac{tp_1}{p_\infty} = 14$

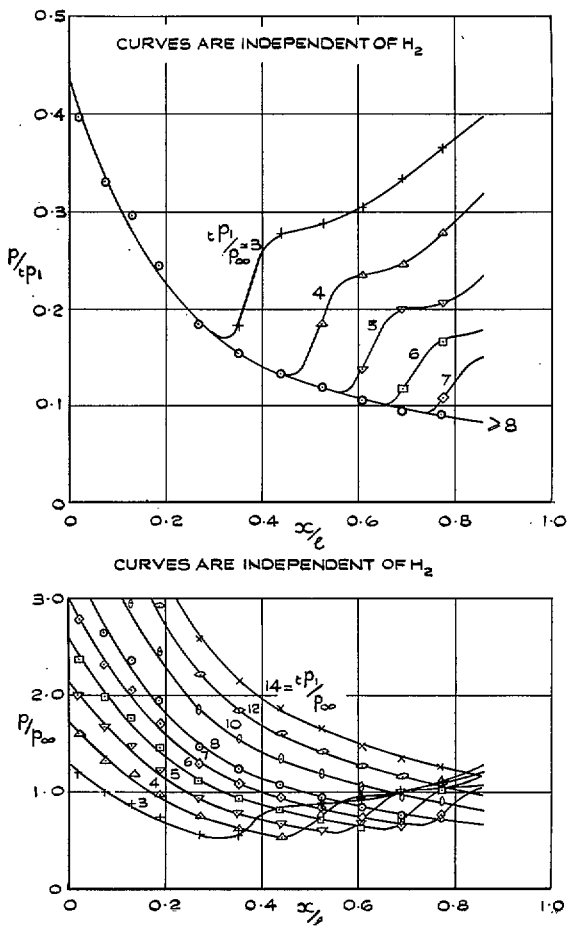

FIG. 24. The effect of jet pressure ratio on the plug pressure distribution. Model No. 1. $M_\infty = 2{\cdot}0$.

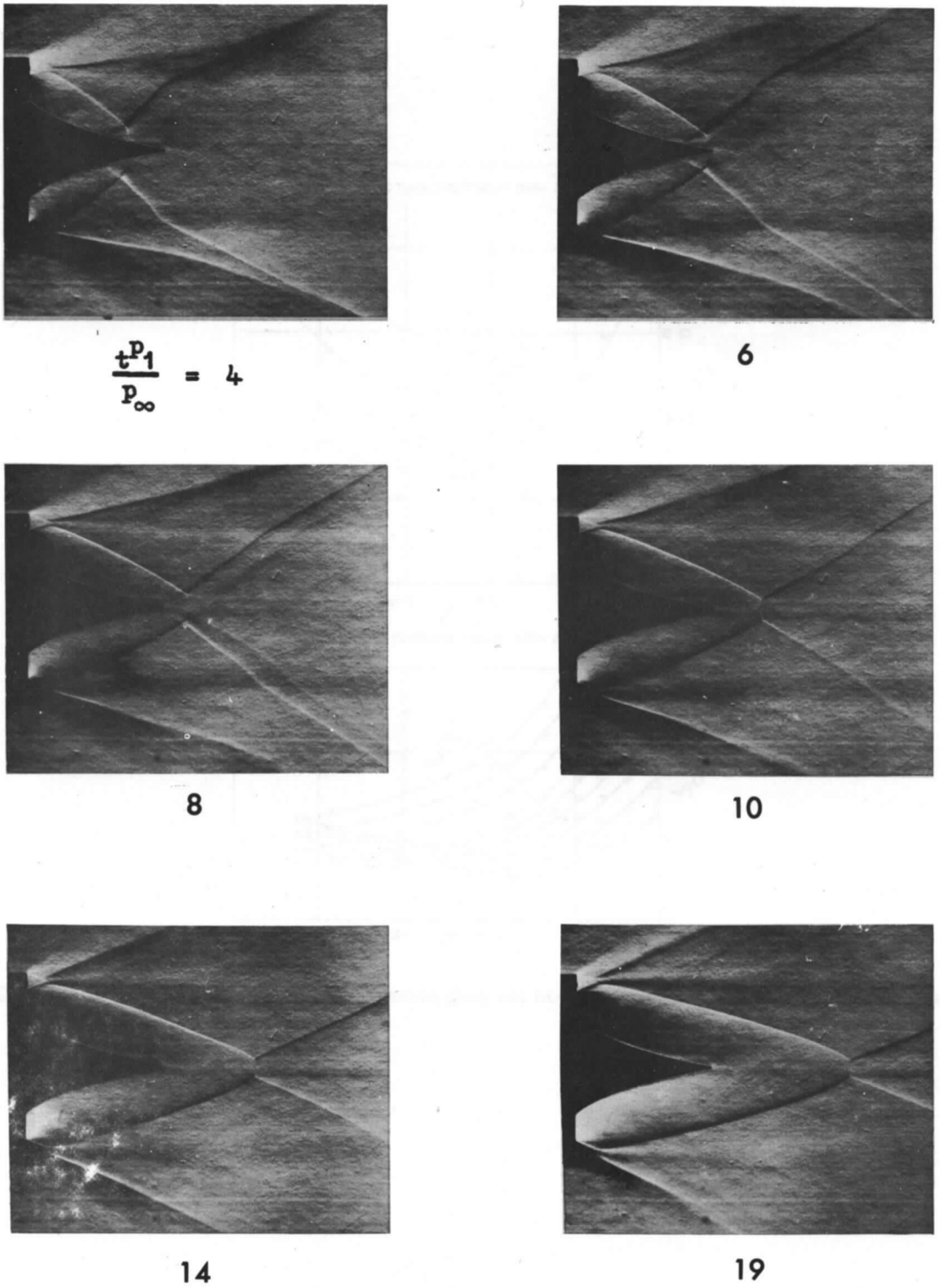

FIG. 25. Schlieren photographs showing the effect of jet pressure ratio on the flow field.
Model No. 1. $M_\infty = 2{\cdot}0$. $H_2 = 0$.

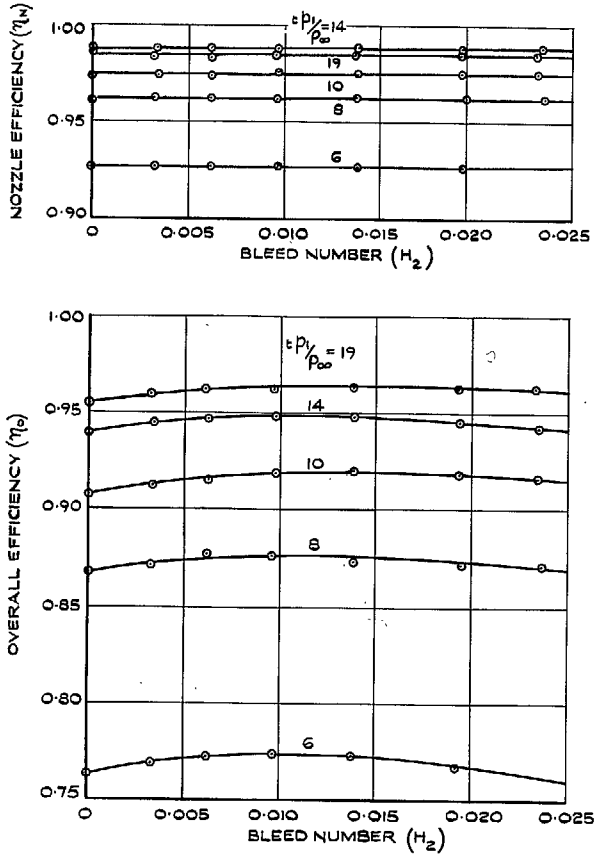

FIG. 26a. The effect of jet pressure ratio and bleed number on the nozzle efficiency and overall efficiency. Model No. 1. $M_\infty = 2{\cdot}0$.

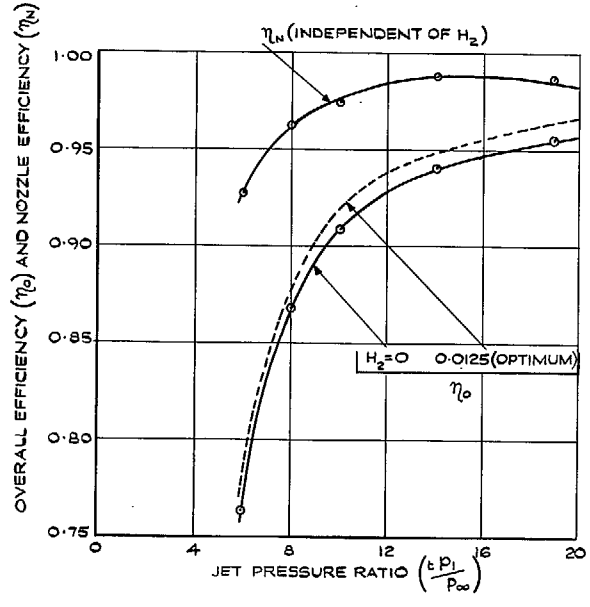

FIG. 26b. The effect of jet pressure ratio and bleed number on the nozzle efficiency and overall efficiency. Model No. 1. $M_\infty = 2{\cdot}0$.

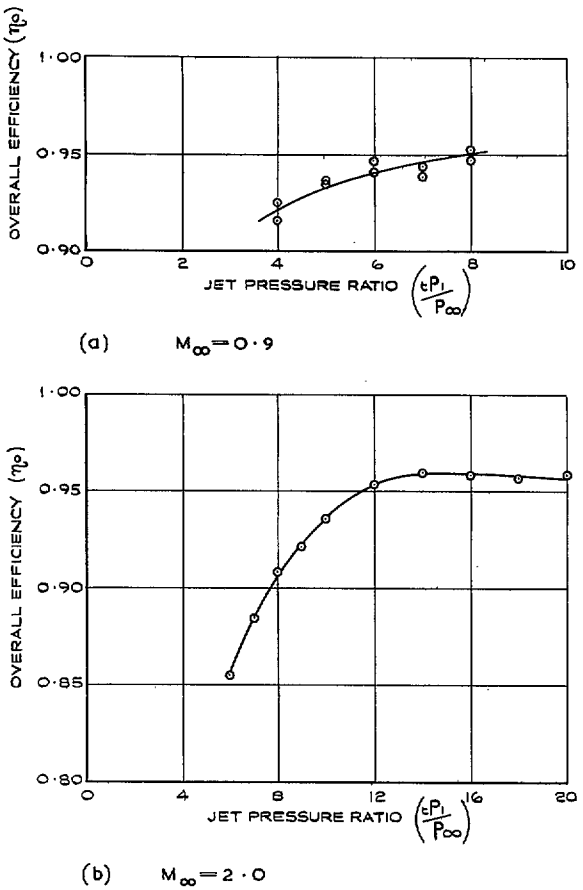

FIG. 27a & b. The effect of jet pressure ratio on the overall efficiency. Model No. 2.

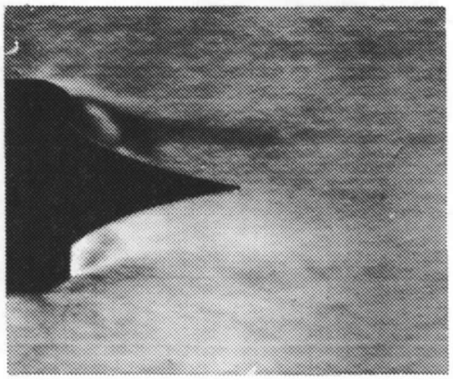

$\frac{t^{p_1}}{p_\infty} = 4$

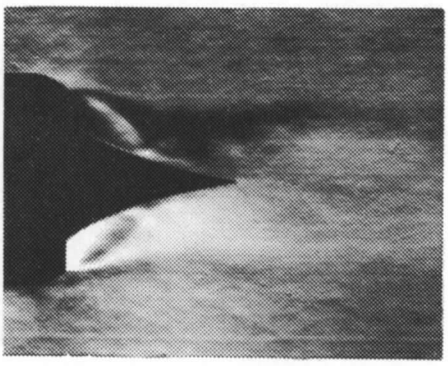

6

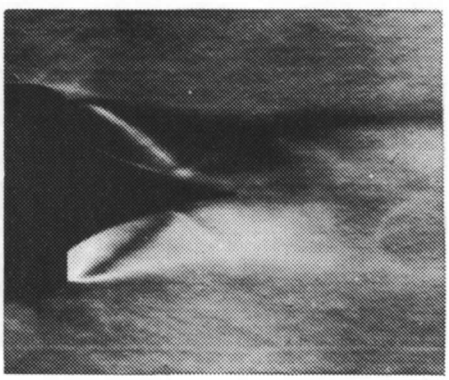

8

FIG. 28. Schlieren photographs showing the effect of jet pressure ratio on the flow field. Model No. 2. $M_\infty = 0{\cdot}9$.

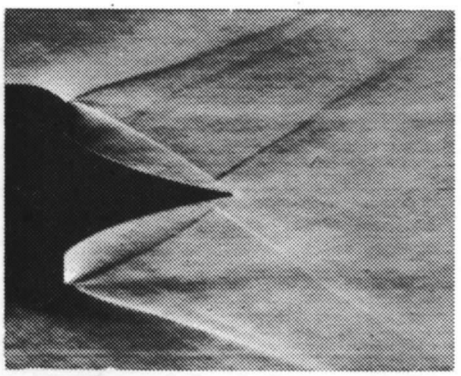

$\frac{t^{p_1}}{p_\infty} = 8$

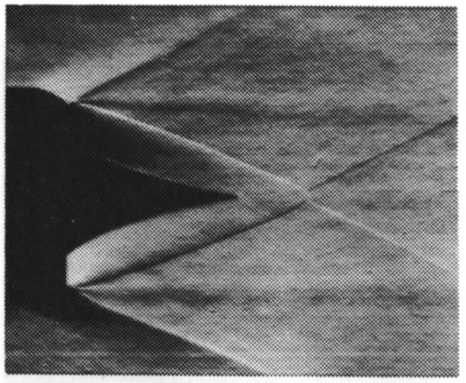

14

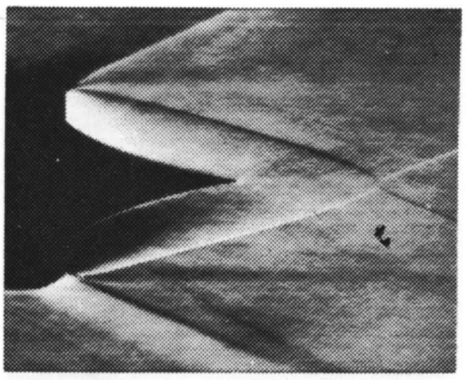

20

FIG. 29. Schlieren photographs showing the effect of jet pressure ratio on the flow field. Model No. 2. $M_\infty = 2{\cdot}0$.

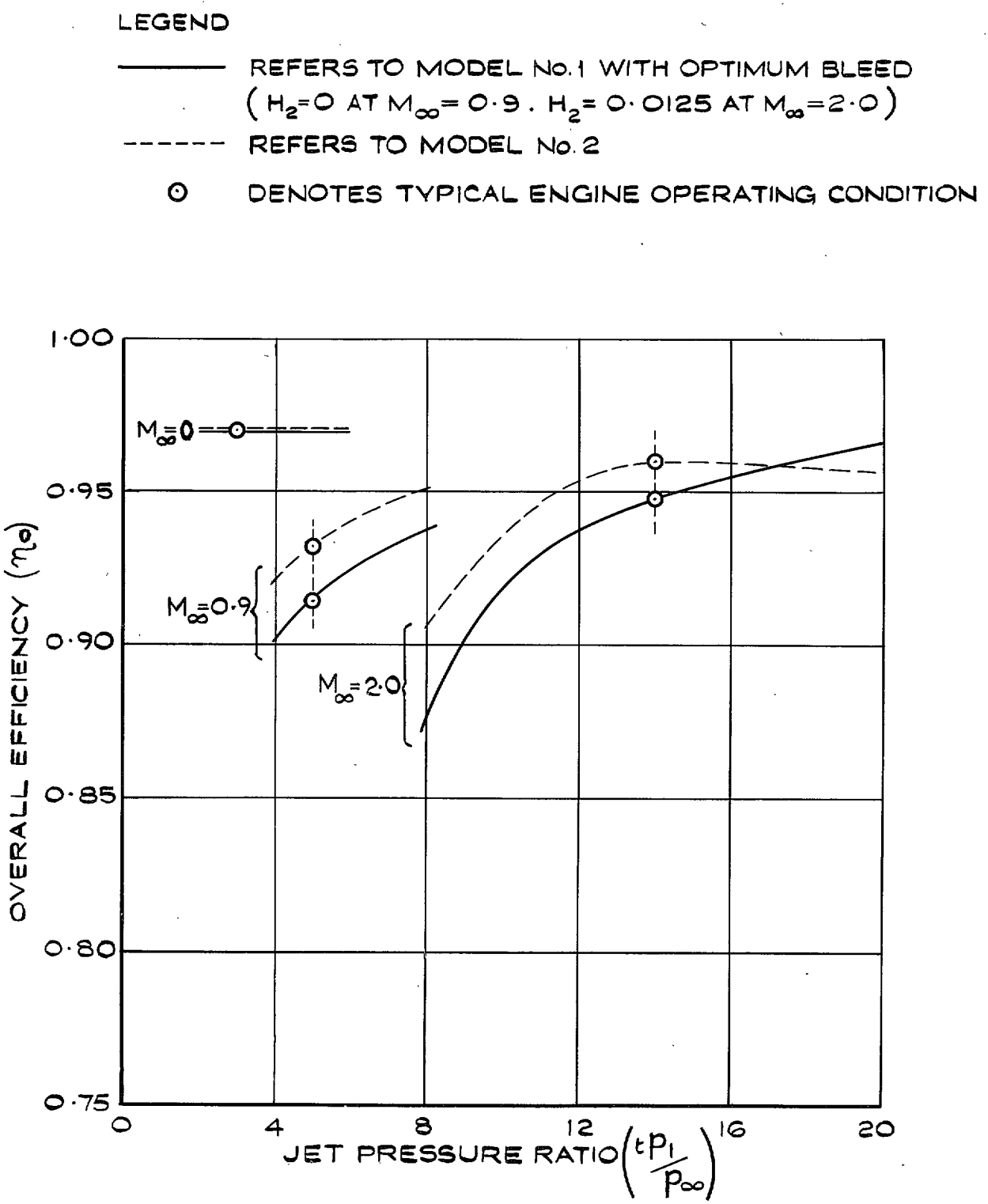

FIG. 30. Comparison of overall efficiency of models No. 1 & 2 with reference to typical engine operating points.

Printed in Wales for Her Majesty's Stationery Office by Allens Printers (Wales) Limited.

Dd.125874 K5 3/67

Published by
HER MAJESTY'S STATIONERY OFFICE

To be purchased from
49 High Holborn, London W.C.1
423 Oxford Street, London W.1
13A Castle Street, Edinburgh 2
109 St. Mary Street, Cardiff
Brazennose Street, Manchester 2
50 Fairfax Street, Bristol 1
35 Smallbrook, Ringway, Birmingham 5
7–11 Linenhall Street, Belfast 2
or through any bookseller

S.O. Code No. 23–3466